A LOW-LEVEL USV CONTROLLER INCORPORATING AN ENVIRONMENTAL

DISTURBANCE OBSERVER

by

Michael Albert Diddams

A Thesis Submitted to the Faculty of

The College of Engineering and Computer Science

In Partial Fulfillment of the Requirements for the Degree of

Master of Science

Florida Atlantic University
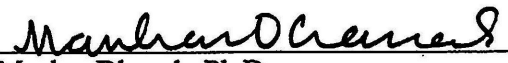
Boca Raton, FL

May 2018

A LOW-LEVEL USV CONTROLLER INCORPORATING AN ENVIRONMENTAL

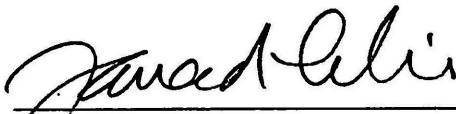DISTURBANCE OBSERVER

by

Michael Albert Diddams

This thesis was prepared under the direction of the candidate's thesis advisor, Dr. Manhar Dhanak, Department of Ocean and Mechanical Engineering, and has been approved by the members of his supervisory committee. It was submitted to the faculty of the College of Engineering and Computer Science and was accepted in partial fulfillment of the requirements for the degree of Master of Science.
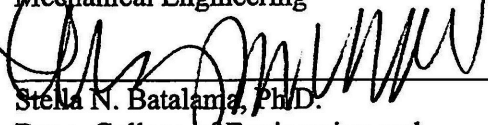
SUPERVISORY COMMITTEE:

_____
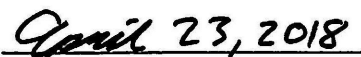Manhar Dhanak, Ph.D.
Thesis Advisor

_____
Betsy Seiffert, Ph.D.

_____
Karl von Ellenrieder, Ph.D.

_____
Javad Hashemi, Ph.D.
Chair, Department of Ocean and
Mechanical Engineering

_____
Stella N. Batalama, Ph.D.
Dean, College of Engineering and
Computer Science

_____
Khaled Sobhan, Ph.D.
Interim Dean, Graduate College

_____
April 23, 2018
Date

iii

ACKNOWLEDGEMENTS

ABSTRACT

Author: Michael Albert Diddams

Title: A Low-Level USV Controller Incorporating an Environmental
                   Disturbance Observer

Institution: Florida Atlantic University

Thesis Advisor: Dr. Manhar Dhanak

Degree: Master of Science

Year: 2018

Modeling, system identification and controller design for a 16' catamaran is described with the objective of enhanced operation in the presence of environmental disturbances including wind, waves and current. The vehicle is fully-actuated in surge, sway and yaw degrees of freedom. Analytical and experimental system identification is carried out to create a numerical model of the vehicle. A composite system of a Multi-input multi-output Proportional-Derivative (PD) controller and a nonlinear disturbance observer is used for station-keeping and transiting modes of operation. A waypoint transiting algorithm is developed to output heading and cross-track error from vehicle position and waypoints. A control allocation method is designed to lower azimuthing frequency and incorporate angle saturation and rate limits. Validation is achieved with improvement in simulation with the addition of the nonlinear observer.

DEDICATION

This manuscript is dedicated to my wife Sarah, my parents, my grandmother and my late grandparents.

A LOW-LEVEL USV CONTROLLER INCORPORATING AN ENVIRONMENTAL

DISTURBANCE OBSERVER

LIST OF TABLES

LIST OF FIGURES

LIST OF EQUATIONS

1 Introduction

This thesis will address automatic control of marine vehicle motion. The motivation for this thesis is improvement in the motion control of unmanned surface vehicles in the presence of environmental disturbances. Rather than only reacting to the feedback error caused by the disturbance, incorporating some knowledge of the disturbance force should reduce position error and conserve energy. Using a passive means to calculate this disturbance, without any extra hardware, can improve an existing control system inexpensively.

1.1 Background

Automatic control of marine vehicle motion has been an active industrial and research field for some time. Some of these technologies have become very widespread in commercial and military use while others, especially systems intended for unmanned operation, have a great potential for future productive value and are an active area of engineering research.

1.1.1 Conventional History

Technology for automatic control of marine vehicle motion has had at least an indirect effect on most humans since the overwhelming majority of us buy or sell goods that have been transported across oceans. A modern manned ocean vehicle will typically be equipped with an autopilot for heading control and an engine speed control system ("governor") that will maintain a specified engine or propeller speed. Dynamic Positioning is a form of automatic motion control used in commercial ships for

maintaining a fixed location in reference to earth with wide applications in the marine petroleum, research, and construction industries. Station-keeping is a more general term that encompasses dynamic positioning. Automatic control systems for following a specified path or trajectory (set using a series of waypoints or a time-based trajectory) are used in specialized commercial applications of manned vehicles and for the control of unmanned vehicles.

1.1.2   Unmanned Surface Vehicles

Unmanned Surface Vehicles (USVs) are an emerging technology with potential uses in surveillance, oceanographic research, and general maritime uses. USVs have the potential to reduce risk to humans in a variety of tasks and have been used in the past for minesweeping and collecting radioactive water samples [1]. In addition, there are major potential cost savings and increased productivity in data gathering and reconnaissance missions.

A USV that is capable of basic semi-autonomous motion operations such as station-keeping and waypoint transiting requires a controller that will use vehicle control elements to maintain position, speed, and/or heading. Control elements can be designed to act using a feedback loop, where the controller responds to error; a feed-forward system, where the control force is adjusted to account for exterior forces; or a combination of both feedback and feed-forward methods. The vehicle heading, speed and position, as well as dynamics which can't be measured directly, are referred to as state. An observer is a method of providing an estimate of some aspect of the state that cannot be measured or improving the measurement of aspects that are measurable. A disturbance

is a change in state not caused by the control system and this includes environmental disturbances caused by wind, waves and current.

System modeling and identification is very useful in controller design and environmental disturbance rejection. A general dynamic, force-based model of marine vehicles is seen in *Guidance and Control of Ocean Vehicles* by T.I. Fossen [2]. This model will be explained in the approach section and will be referred to in this paper as *the dynamic model*.

1.2   Equipment

This thesis addresses the design of an automatic motion control system for one specific combination of vehicle and propulsion system: The WAM-V USV 16 and Torqeedo Cruise 2.0 R thrusters. Both components, and this combination, are in commercial production, which gives a control system designed for their use a wide possibility of applications. The custom designed guidance, navigation and control system will also be discussed.

1.2.1   The WAM-V USV 16

The USV which will be referenced in this thesis is a 16' long Wave Adaptive Modular Vehicle (WAM-V) made by Marine Advanced Research of Richmond, California. This catamaran style vehicle is designed with a suspension system that allows pontoon style hulls to rise and fall in waves while maintaining stability of a center payload tray.

1.2.2   Torqeedo Cruise 2.0 R

The vehicle is equipped with two 2 kW Torqeedo electric motors that can be used for differential thrust steering and azimuth steering. The manufacturer estimates that

these motors are equivalent to a 5HP (3.7 kW) gas-powered outboard motor in terms of propulsive power due to greater efficiency in drive train and propeller [3]. The motors are powered by two Lithium Nickel Manganese Cobalt Oxide (Li NMC) Power 26-104 batteries, also manufactured by Torqeedo. Both the motors and batteries are equipped with electronic safety systems which will limit power output and protect the batteries from deep discharge and overheating, among other features [4].

1.2.3   Performance Characteristics

The vehicle has been tested at a maximum surge speed of 5.7 m/s (11.1 knots) which results in a Froude number of 0.825. At speeds above 2.8 m/s, the vehicle is in the semi-planing speed range which indicates that there will be a crest of water at the bow of the vessel [5]. Given the vehicle's round hull-forms, it is expected that drag will increase nonlinearly at speeds above this point.

1.2.4   Guidance, Navigation and Control System

A custom Guidance, Navigation and Control (GNC) system was built for the USV that allows for programmed missions or radio control [6]. The Torqeedo motor and battery system use a Propulsion Control Unit (PCU) to control motor speed and actuators for azimuthing. The PCU accepts Pulse-Width-Modulation (PWM) inputs from a PixHawk 2.1 microcontroller or the radio control receiver via an adapter that linearly relates the PWM to motor speed and azimuthing actuator position commands. The PixHawk is implemented with the HERE+ sensor unit which includes an RTK GNSS system (i.e. Global Positioning System, GPS) and MPU9250 accelerometer/magnetometer/gyroscope (i.e. Inertial Measurement Unit, IMU). An ODRIOD-XU4 (an ARM based computer) within the control box and a Wi-Fi router

allows use of a ground control station to plan, save, and load autonomous missions (using a point-and-click interface for waypoint missions) and download mission logs.

The PixHawk and ODROID, like the Torqeedo thrusters, are available to consumers, increasing the potential usefulness of a system designed with this platform.

Figure 1-1: WAM-V in testing operation at SeaTech

2   Problem Statement and Thesis Objectives

The research community is tasked with improving the motion control of unmanned surface vehicles particularly when they are in autonomous mode. When these vehicles are in operation on the sea they will be exposed to environmental disturbances and will typically not have any information on the nature of those disturbances other than sensor data such as position and velocity from a GPS and IMU. While a human operator may use intuition and experience to reject disruptions to motion control from environmental forces, an unmanned surface vehicle will have a more basic set of tools and will need to make decisions of what control forces to apply and how to apply them quickly, reliably and in a way that ensures stability. A control system using a nonlinear observer together with a feedback controller will be designed to improve motion control of unmanned surface vehicles and will be tested using simulation.

This thesis will address the following objectives:

- Design a nonlinear state observer with inputs of vehicle dynamics from sensors and control force from thrusters to estimate disturbance forces acting on the vehicle, presumed to be wind, waves and current to be used with a proportional-derivative (PD) controller with an input of state error from a desired position or trajectory. A diagram of the observer-controller system is seen in Figure 2-1.

- Command the control system to undertake station-keeping and waypoint-following missions and simulate the vehicle exposed to environmental

disturbances from wind, waves and current. Quantify effect of observer on control system by comparison with control system without observer.

The simulations used for validation will be of station-keeping at a fixed point and transiting in a "lawnmower" pattern because of their usefulness in unmanned operations. The lawnmower pattern can be used with side-scan sonar to map the sea floor and detect undersea objects such as marine life and naval mines. Station-keeping is useful in monitoring variable conditions such as water depth, temperature and salinity as well as wind and current speed.
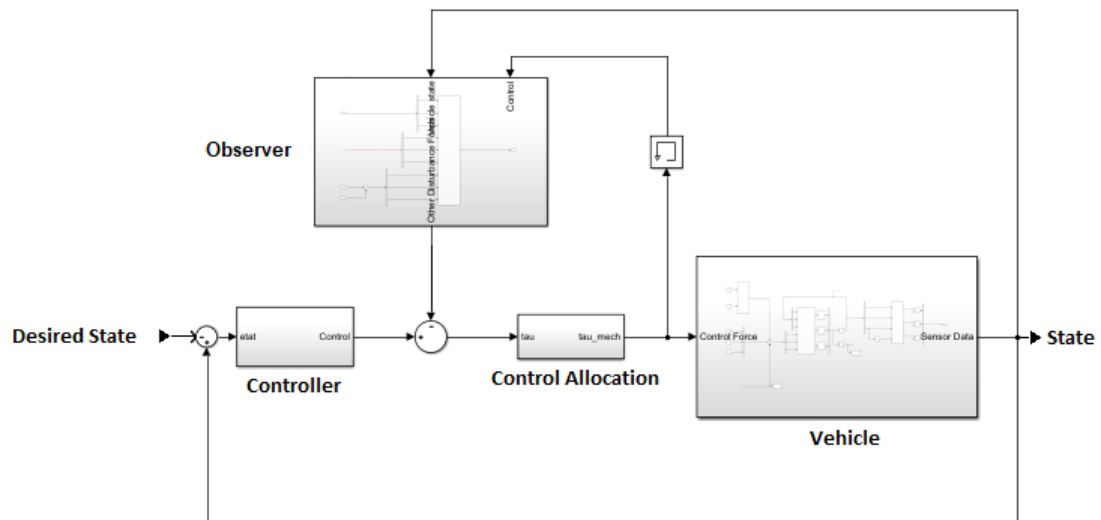
Figure 2-1: Control system diagram

3 Literature Review

Environmental disturbance rejection is an important and hotly discussed topic in USV controller design [7]. USVs are often much lighter than ships for which controllers have historically been designed and can thus be very vulnerable to environmental disturbances. A model to convert wind speed and direction to three degree of freedom force on a ship is seen in *Fossen* [2], and this has been implemented using a vehicle mounted weather station with success by Qu et al. [8] [9]. The primary research contribution of this thesis is expected to be environmental disturbance rejection using a nonlinear state observer. The following literature review will elaborate on the reasons to use such a method, keeping in mind improved performance in the presence of wave and current force.

3.1 Dynamic Systems and State Vectors

A marine vehicle is a dynamic system, changing over time in a way that can be approximated by fixed equations. A general dynamic system approximated by a first-order differential equation is as follows:

$$\dot{x} = f(x(t), u(t), t) \tag{1}$$

Here, x is the system state vector (in this case, vehicle velocity is a candidate), u is control input (force from thrusters) and t is time [10]. If the initial condition is known, the state can be found by integrating this dynamic model over time. A dynamic system with a feedback controller is modeled in the following diagram:
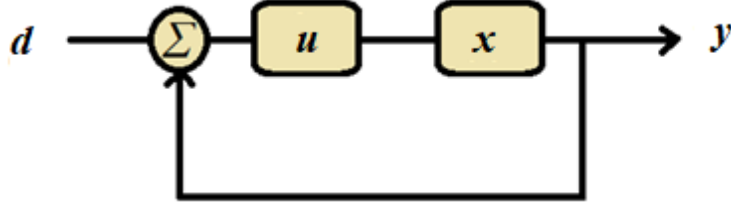
Figure 3-1: Dynamic system with feedback control

in which *d, u, x* and *y* represent desired state, control input, state and output respectively.

The output, *y*, represents measurable aspects of the state and is influenced by sensor error

and noise. An observer is designed to estimate parts of the state that are not measurable,

stated generally: "Given a system described by a representation

$$\dot{x}(t) = f\big(x(t), u(t)\big) \tag{2}$$

$$y(t) = h(x(t)) \tag{3}$$

find an estimate *x̂(t)* for *x(t)* from the knowledge of *u(τ), y(τ)* for $0 \le \tau \le t$." [11]

3.2   State Observers

The components of state that are measurable and that need to be estimated by an

observer vary from system to system. Kalman filtering has been used for increasing

accuracy in position measurement by combining data from accelerometers and GPS using

a prediction-correction algorithm to achieve accuracy and detect small motions [12] and

for estimating velocity with only heading and position sensors [13]. This is a form of

observer intended primarily to account for error and noise in sensors because position and

velocity could be measured directly using only GPS data.

3.2.1   Disturbance Observer Based Control

Chen et al. [14] refers to a control system incorporating a disturbance observer as

Disturbance Observer Based Control (DOBC). Such systems have been developed by

engineers independently since the 1960s in a variety of fields and for linear (which may use frequency domain) and nonlinear systems. A method to solve for disturbances in slowly varying systems was developed in 2000 in [15] to be used for nonlinear friction in robotic manipulator joints. A simple model of DOBC is seen in Figure 3-2, inspired by [16]. A control system incorporates the disturbance in a composite form by feeding the estimated disturbance through a separate controller and summing this with the output of the feedback controller in the form:

$$u = u_f + u_d \tag{4}$$

or by simply summing the estimated disturbance with the feedback controller output in the following form:

$$u = u_f + \hat{d} \tag{5}$$
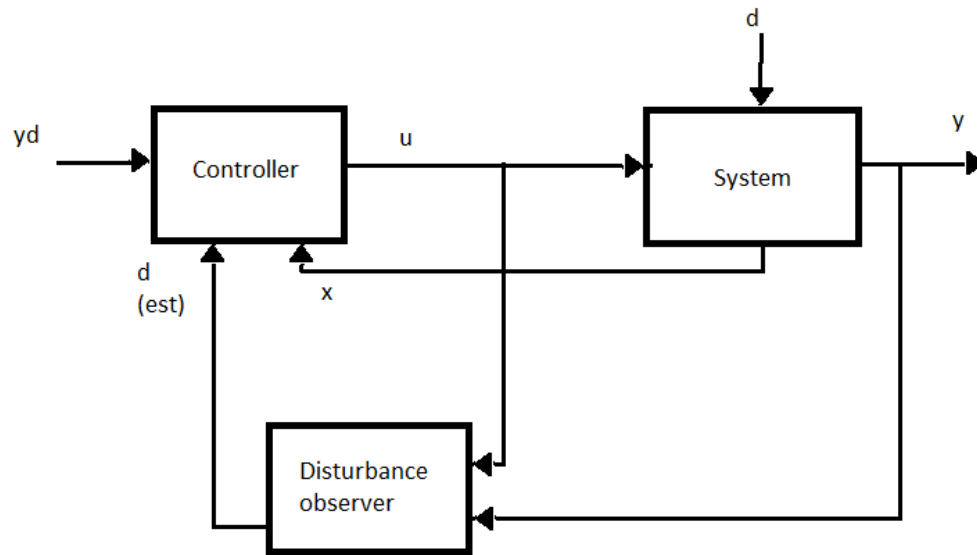
Figure 3-2: Simple DOBC diagram

K. Do (2010) describes a general nonlinear observer in the following form:

$$\dot{x}_1 = F_1(x_1, x_2) \tag{6}$$

$$\dot{x}_2 = F_2(x_1, x_2, u) + G(x_1)d(t) \tag{7}$$

$$\hat{d}(t) = \xi + K_0 G^{-1}(x_1)x_2 \tag{8}$$

$$\dot{\xi} = -K_0\xi - K_0(\dot{G}^{-1}(x_1)x_2 + G^{-1}(x_1)F_2(x_1, x_2, u) \tag{9}$$
$$+ K_0 G^{-1}(x_1)x_2)$$

The state is expressed as two variables, x_1 and x_2, that are possible to model through functions F_1 and F_2, as well as the unmodelled part $d(t)$ [17]. In this thesis x_1 will be position, x_2 will be velocity and $d(t)$ will be the disturbance force. K_0 is a matrix from which the eigenvalues determine the gain of the observer (how aggressively it converges) and u is the control thrust input to the system.

3.3   Nonlinearity and Lyapunov Stability Theory

A dynamic model of a marine vehicle will typically include some nonlinear parameter. This is easiest to see in the hydrodynamic drag, where a vehicle with a displacement style hull will see exponential increases in drag as speed increases above very slow speeds. Powerful tools for analyzing and controlling linear systems were developed during the 20th century which allow an effective linear controller to be designed to stabilize these systems. Because these tools can be ineffective in analyzing nonlinear systems, other methods are needed to ensure stability [18].

The observer described in *Do* utilizes the parameters from the dynamic vehicle model in function F_2, but these parameters do not need to be accurate for the state observer to be able to calculate the disturbance force because the model is exponentially

stable: the estimated disturbance force will exponentially converge to the actual disturbance force. The observer is derived using the following Lyapunov direct method and function.

$$V_e = \frac{1}{2} d_e^T d_e \qquad (10)$$

Here, d_e is the error of the disturbance observer. This function is analogous to the kinetic energy equation and when used with the equations (8, 9) d_e will converge to zero if the disturbance force d is constant.

3.4   Controller Types

This section will describe various types of controllers that have been used in unmanned marine vehicles.

3.4.1   Model Based Control

Fed forward model-reference force has been used in surface vehicle controllers and combined with fed forward wind force in Sorenson et al. (1995) [19]. In this form of fed forward control, a desired velocity and acceleration are inserted into the dynamic model and a corresponding force is calculated and fed forward. This force is combined with a linear-quadratic-Gaussian (LQG) feedback controller, fed forward wind force from a weather station, and parallel independent control for disturbance rejection. This controller was successfully implemented on a 4200-deadweight-ton offshore supply vessel.

Nonlinear control methods such as backstepping and sliding mode control will typically include parameters from the dynamic model in the control law, and these will be addressed in their respective sections.

The backstepping and sliding mode controllers described in Klinger et al. (2017) [20] are significant in that they employ an adaptive method to modify dynamic model parameters within the control law for use with autonomous launch and recovery missions with an Autonomous Underwater Vehicle (AUV). The parameters were adaptively tuned using the direct Lyapunov method so that error in these terms would converge to zero. Experiments showed that this adaptive backstepping controller was able to significantly reduce steady-state error in speed and heading, although it resulted in larger errors in the transient stage immediately after launching the AUV.

3.4.2 *Backstepping control*

Fossen and Strand define nonlinear backstepping as a "recursive design methodology for the construction of both feedback control laws and associated Lyapunov functions in a systematic manner" [21] and describe a three degree of freedom vectorial backstepping method which is used in the backstepping controller described by Sarda et al. in [22] (2015). It was found it to be more precise than a PD controller or sliding mode controller under similar circumstances. It uses a Lyapunov function like that used in the Do observer.

For underactuated transiting, Bertaska et. al. [23] (2015) and Do use backstepping methods described by Khalil (2002) [18]. Klinger et. al. uses a feedback linearization technique described by Slotine and Li [24] (1991). The system used in Sarda et. al. for fully actuated station-keeping [22] could not be applied directly in an underactuated system because of the absence of controlled sway force.

3.4.3 Sliding mode control

Sliding mode control is explained by Slotine and Li in the context of a surface, *s*, created as a function of state and time. When the state reaches this surface, it is forced to stay on it; thus, it slides. Sarda et. al. used this method in station keeping and found it to be the most robust in maintaining heading.

3.4.4 Proportional Integral Derivative (PID) control

PID control is used in a vast number of industrial applications. Engineers working for Honeywell have stated that "Based on a survey of over eleven thousand controllers in the refining, chemicals and pulp and paper industries, 97% of regulatory controllers utilize PID feedback" [25]. It is a widely taught and understood control process among industrial technicians: a signal of error for a given controlled output is fed in parallel through proportional, integral and derivative blocks which leave this signal unchanged, integrate the signal over time and take the derivative of the signal over time, respectively. The effect is to act on the error directly through proportional action, act on the history of the error through integral action and act of the expected future of the error through derivative action. The controller is tuned with a gain for each of the blocks which are then summed to create the control input.

There is no reason that a PID controller cannot be used for nonlinear systems, but there is a great advantage to using a linear (or linearized) model to design and tune a PID controller so that transfer functions of the system may be easily used [26]. A PD controller is used in Sarda et. al. [22] which has the advantage of not requiring vehicle dynamic model parameters to be used as part of the control law and the ability to operate neatly in vectorial format. This type of controller will be used for station keeping in this

thesis because of its wide use and simplicity. The design of a PID controller, especially for a nonlinear system, can be made easier by employing self-tuning gains through methods such as fuzzy logic and artificial neural networks.

Fuzzy Logic was proposed in 1965 by Lotfi Zadeh as an alternative to Boolean logic, so that rather than classifying a conclusion as true or false it can be "somewhat true" or "somewhat false". Fuzzy logic has been used with a self-tuning PID controller for an autonomous underwater vehicle by M. Hammad [27] in which fuzzy rules are set based on an engineer's intuition in tuning PID gains: the error and error derivative are measured and, for example, the P-gain will be increased if there is a large, slowly varying error. This increase will be in proportion to how large the error is and how slowly it varies.

Artificial neural networks are an artificial intelligence system inspired by biology and named for the neurons in an animal brain. A form of artificial neural network known as Artificial Bee Colony (ABC) is used by Yang et. al. [28] to tune PID gains for an unmanned surface vehicle. Error between outputs of a reference model and the vehicle are fed to the ABC as a form of feedback control in which the ABC reduces the error between the reference model and vehicle by tuning the PID gains.

3.5 Modeling and System Identification Techniques

Modeling and system identification is a very important topic in controls which becomes more complex as higher speeds and nonlinearities are introduced. There are various methods to obtain a model of a marine vehicle, involving different degrees of *a priori* knowledge of system parameters. Once system identification has been conducted, a simulation should be possible in which an experimental vehicle trajectory is overlaid on a

15

simulated trajectory (given only control and environmental inputs) and error between the two can be measured.

As mentioned in the Background section, a general model presented by Fossen is very effective because it can be used in a vectorial format and incorporates linear and nonlinear terms in six degrees of freedom if necessary [2]. He also presents methods to calculate the drag and added mass coefficents used in this model.

Using an autonomous ridged hull inflatable boat, Sonnenburg and Woolsey [29] developed a model that incorporated scheduled conditions for displacement, semi-displacement and planing conditions with linearization. This vehicle was underactuated with one steerable outboard motor and the Nomoto model was used to obtain steering dynamics with incorporation of sideslip.

An experimental approach was used by Elkaim [30] for heading control of a sailing catamaran. This approach uses Observer Kalman filter IDentification (OKID) and assumes a linear time invariant system, of which it tunes the state, input and output matrices.

In 2002 the International Maritime Organization instituted requirements for commercial ships to meet maneuvering standards by performing four tests: straight line, zig-zag with 10º rudder, zig-zag with 20º rudder and circle with 35º rudder [31]. The purpose of these test is to ensure that a ship meets minimum standards for maneuverability and stability, but tests based on this are also used with unmanned vehicles because they are able to incorporate most or all of the coefficients used in a dynamic model and validate the accuracy of that model [20] [32] [29].

3.6   Control Allocation

Control allocation is the method of converting forces in three degrees of freedom to actuator commands. Control allocation for a fully-actuated marine vehicle with two stern-mounted azimuthing thrusters can be accomplished in multiple ways. Fossen and Johansen (2006) [33] describe linear quadratic unconstrained, linear quadratic constrained and nonlinear constrained methods, of which the linear quadratic unconstrained is the most straight-forward but does not provide a built-in solution for constraints of thrust and azimuth angle. Johansen et al. (2008) [34] gives an explicit solution for azimuthing thrusters with angle constraints with piecewise linear functions and Johansen (2004) [35] provides a nonlinear constrained allocation method using a Lyapunov approach, both of which use cost functions for optimization.

Sordanlen [36] uses a method to optimize for minimal azimuthing movement in dynamic positioning without relying on statistical optimization methods by using an algorithm where an angle is selected to satisfy the force command from the controller, then low-pass filtered to eliminate high frequency turning, then used to calculate required thrusts using linear algebra. This method is attractive because it accomplishes reducing wear and oscillations of actuators as well as introducing the possibility of incorporating rate limitations and saturation of azimuth angle without requiring a cost function.

4   Approach

The work of this thesis includes the full cycle of controller design, starting with modeling, system identification testing and open loop simulation and concluding with design of a controller, disturbance observer, control allocation method and waypoint-tracking algorithm for the transiting controller. The original intent of this thesis was to implement the designed components using PixHawk microcontroller programmed in C++ and performing tests on inland waterways, but this was reduced to simulation of the control system, vehicle and environmental disturbances using Matlab/Simulink. This section will be broken into three parts: modeling and system identification, controller design and simulation, and validation through simulation.

4.1   Modeling and System Identification

The vehicle and the wind, wave and current forces acting on it are modeled in three degrees of freedom, including the key step of system identification and construction of the dynamic model.

4.1.1   *Reference Frames*

The frame of reference must be kept in mind always during this process. We will use the body fixed system, in which the origin is located at the vehicle center of gravity and the x-axis extends directly forward along the centerline in the surge direction (through the bow, if this were a monohull ship), the y-axis from the center of gravity directly starboard in the sway direction and the z-axis from the center of gravity directly downwards in the heave direction. Rotation about the z-axis is in accordance with the

18

right-hand rule and called yaw. We will deal only in three degrees of freedom and ignore

heave, roll and pitch motions. This is illustrated in Figure 4-1.
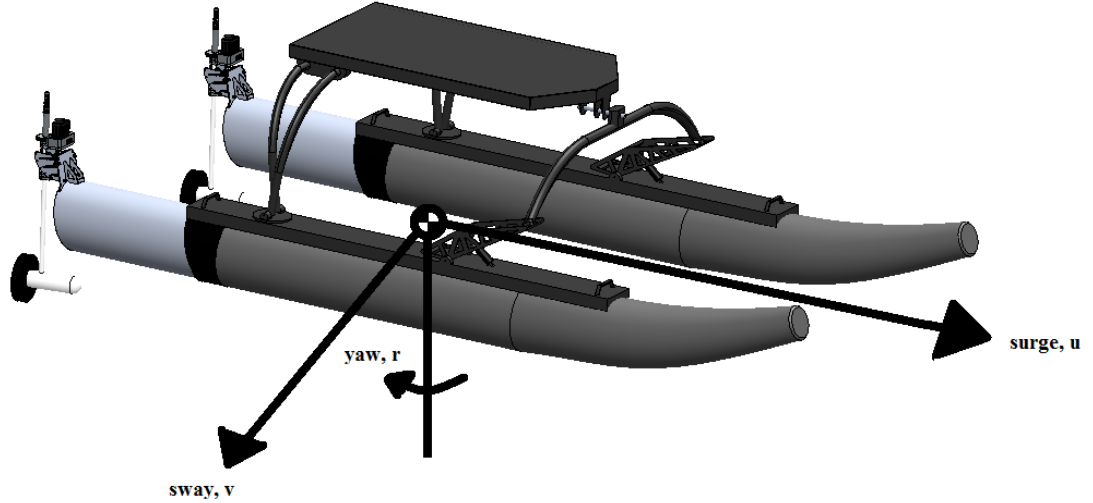
Figure 4-1: Body-centered frame of reference

We will also use the earth fixed system referred to as North-East-Down (NED) in

which the axes are centered at an arbitrary point on the ocean surface with the x-axis

extending directly northwards, the y-axis extending directly eastwards and the z-axis

extending directly downwards.

In the body-fixed coordinate system velocities are represented as *u, v, r* and forces

as X, Y, N in the surge, sway and yaw direction, respectively. ψ (psi) is heading, per the

right-hand rule, from north.

$$\eta = [x, y, \psi]^T \; for \; earth \; fixed \; position, \tag{11}$$

$$v = [u, v, r]^T \; for \; body \; fixed \; velocity, \tag{12}$$

$$\tau = [X, Y, N]^T \; for \; body \; fixed \; force \tag{13}$$

Transformation between the body and earth fixed frames can be accomplished
through:

$$\dot{\eta} = J(\eta)v \tag{14}$$

$$v = J^T(\eta)\dot{\eta} \tag{15}$$

$$J(\eta) = \begin{bmatrix} \cos(\psi) & -\sin(\psi) & 0 \\ \sin(\psi) & \cos(\psi) & 0 \\ 0 & 0 & 1 \end{bmatrix} \tag{16}$$

4.1.2 Dynamics

Vehicle motion is expressed with a balance of body-fixed forces from Newton's second law, hydrodynamic damping, Coriolis force, control forces and environmental forces. These forces may be modelled in vectorial form using the following form (from Fossen [2]):

$$M\dot{v} + C(v)v + D(v) = \tau_{control} + \tau_{env} \tag{17}$$

$$M \equiv mass\ matrix, C(v) \equiv Coriolis\ matrix,$$

$$D(v) \equiv drag\ matrix,$$

$$\tau_{conrtol} \equiv control\ force\ vector$$

$$\tau_{env} \equiv environmental\ force\ vector$$

$$M = \begin{bmatrix} m - X_{\dot{u}} & 0 & 0 \\ 0 & m - Y_{\dot{v}} & -Y_{\dot{r}} \\ 0 & -N_{\dot{v}} & I_z - N_{\dot{r}} \end{bmatrix} \tag{18}$$

$$C(v) = \begin{bmatrix} 0 & 0 & -(m - Y_{\dot{v}})v + \dfrac{Y_{\dot{r}} + N_{\dot{v}}}{2}r \\ 0 & 0 & (m - X_{\dot{u}})u \\ (m - Y_{\dot{v}})v - \dfrac{Y_{\dot{r}} + N_{\dot{v}}}{2}r & -(m - X_{\dot{u}})u & 0 \end{bmatrix}, \tag{19}$$

$$D = -\begin{bmatrix} X_{|u|u}u + X_u & 0 & 0 \\ 0 & Y_v & Y_r \\ 0 & N_v & N_r \end{bmatrix}. \tag{20}$$

Gravity effects are not included here because of the exclusion of heave, pitch and roll.

The mass, Coriolis and drag matrices are expressed using SNAME 1950 notation in which a term's position in the matrix corresponds to the force produced in the body fixed direction denoted by the term's matrix row, for motion in the body fixed direction denoted by the term's matrix column.

The mass matrix includes both the ridged body terms of mass and moment of inertia and added mass terms corresponding to the inertia of the surrounding fluid. The drag matrix is a damping term consisting of radiation-induced potential damping (energy dissipated by wave generation), skin friction, wave drift damping and damping due to vortex shedding. Because we are in the body-fixed frame of reference, the Coriolis matrix (also called Coriolis and centripetal matrix) shows forces that appear due to the rotation of the body-fixed frame with respect to the inertial frame (all the Coriolis terms are either caused by rotation or would cause a rotational force).

The dynamic model may also be expressed in non-vectorial form (force = τ = [X, Y, N]^T):

$$X = \dot{u}(m - X_{\dot{u}}) + u(X_u + X_{uu}u) - r\left(Y_{\dot{v}}v + mv - \frac{r(N_{\dot{v}} + Y_{\dot{r}})}{2}\right) \tag{21}$$

$$Y = \dot{v}(m - Y_{\dot{v}}) - Y_{\dot{r}}\dot{r} + Y_r r + Y_v v + r(X_{\dot{u}}u + mu) \tag{22}$$

$$N = \dot{r}(I_z - N_{\dot{r}}) - N_{\dot{v}}\dot{v} + N_r r + N_v v + u\left(Y_{\dot{v}}v + mv + \frac{r(N_{\dot{v}} + Y_{\dot{r}})}{2}\right) \qquad (23)$$

$$- v(X_{\dot{u}}u + mu)$$

This can be rearranged in terms for the differential equations for acceleration:

$$\dot{u} = \frac{X + r\left(Y_{\dot{v}}v + mv - \frac{r(N_{\dot{v}} + Y_{\dot{r}})}{2}\right) - u(X_u + X_{uu}u)}{(m - X_{\dot{u}})} \qquad (24)$$

$$\dot{v} = \frac{Y - r(X_{\dot{u}}u + mu) - Y_v v + Y_{\dot{r}}\dot{r} - Y_r r}{(m - Y_{\dot{v}})} \qquad (25)$$

$$\dot{r} = \frac{N + N_{\dot{v}}\dot{v} - N_v v - u\left(Y_{\dot{v}}v + mv + \frac{r(N_{\dot{v}} + Y_{\dot{r}})}{2}\right) + N_r r + v(X_{\dot{u}}u + mu)}{(I_z - N_{\dot{r}})} \qquad (26)$$

4.1.3   Model Simplification

A significant modification is made to the model by decoupling the surge mode from yaw and sway modes, eliminating several drag and added mass terms. Assuming vehicle symmetry, only diagonal ridged body mass terms are present. Looking at the non-vectorial dynamic model, forward motion is not affected by sway velocity and vice-versa unless the vehicle is also rotating.

4.1.4   System Identification

With the equations of motion in (17) and their elaboration in (18-20) we are left with the task of determining the terms in these equations analytically or empirically. Earth fixed position and body fixed velocity are assumed to be collected by vehicle sensors, but body fixed thrust forces and moments are typically not directly known. Generally, the added mass terms are calculated using strip-theory for slender bodies, in which the submerged portion of the hulls are divided into strips for which hydrodynamic

coefficients are calculated and summarized over the length of the body. Mass can be calculated from manufacturers specifications and moment of inertia be calculated using parallel axis theorem, which can be implemented using a CAD program. Drag terms due to potential damping and damping due to vortex shedding may be estimated using experimental data for these terms using floating cylinders.

This thesis will not address the analytical calculation of added mass and drag terms, but rather will use a combination of previously published added mass and drag terms tuned using open loop simulation combined with some directly determined terms. The bollard-pull test, to determine a relationship between static thrust and propeller speed, is the first step to the open loop system identification process followed by a straight-line test to determine linear and non-linear surge direction drag terms, circle tests with wide and tight radii to determine sway and yaw direction drag terms and a zig-zag test to validate added mass terms.

The system identification tests were conducted in North Lake, Hollywood, Florida on February 27th, 2017. Wind was present and was likely to have affected the results. Due to the high speeds are large areas over which the tests took place, the goal of the open loop simulation and tuning process is to match the approximate shape of the experimental trajectory rather than to duplicate it exactly.

Although the vehicle can operate in a fully actuated configuration, the system identification tests were conducted in an underactuated configuration, with each thruster oriented directly forward.

Due to the need for critical analysis, system identification test results will be presented in the results section.

4.1.4.1 <u>Thrust Model</u>

Marine vehicle thrust has been modelled as either a linear function of propeller speed [20] or as a function of both forward velocity and propeller speed, with a linear relation to forward speed and a quadratic relation to propeller speed. Both models and the process for deriving them will be explained here.

For both models, a bollard pull test is needed to find the static thrust of the vehicle, with the goal of mapping known values such as propeller speed and forward velocity to thrust produced by control elements. An eye-bolt was driven into a piling on the SeaTech (Florida Atlantic University at Dania Beach) marina quay, to which a linear scale was attached. A rope from the linear scale went through a pulley attached to the vehicle and then back to the piling to double the range of the scale.

4.1.4.1.1 Linear model

$$T_{wj} = \frac{n}{n_{max}} * T_{max} = An \tag{27}$$

$$T_{wj} \equiv static\ thust, n = propeller\ speed$$

$$n_{max} \equiv maximum\ propeller\ speed, T_{max} \equiv maximum\ thrust$$

$$A \equiv static\ thrust\ coefficient \equiv \frac{T_{max}}{n_{max}} \tag{28}$$

This model has the advantage of only requiring one bollard pull test to construct and knowledge of the propeller speed to implement.

4.1.4.1.2 Nonlinear model

For an alternate model we start by observing that J. N. Newman in *Marine Hydrodynamics* [37] nondimensionalizes propeller thrust:

$$\frac{T}{\rho n^2 d^4} = K_T(J) \tag{29}$$

$$J = \frac{U}{nd} \tag{30}$$

$$T \equiv thrust, \rho \equiv density, n \equiv \frac{revolutions}{time\ unit},$$

$$d \equiv propeller\ diameter, \quad U \equiv forward\ velocity$$

The nondimensional coefficient K_T is observed to typically be a linear function of the advance ratio J [38], such that:

$$K_T(J) = \alpha_2 - \alpha_1 J \tag{31}$$

$$T = \alpha_2 \rho n^2 d^4 - \alpha_1 U \rho n d^3 \tag{32}$$

Here, α_1 and α_2 are constant coefficients. Grouping together constant terms and changing sign of α_1 results in the following:

$$T = a_1(\rho d^3)Un + a_2(\rho d^4)n^2 \tag{33}$$

This shows a quadratic, rather than linear, relation of thrust to propeller speed in addition to a linear relation to propeller forward velocity.

To solve for the coefficients a_1 and a_2 we first use the results of the experimental bollard pull (static thrust) test and set $U = 0$:

$$a_2 = \frac{T}{(\rho d^4)n^2} \tag{34}$$

It is more difficult to solve for coefficient a_1 given that we do not have a way to measure thrust while the vehicle is moving. If this information was obtained, either directly or through approximations from other sources a_1 could be calculated.

$$a_1 = \frac{(T - a_2(\rho d^4)n^2)}{(\rho d^3)Un} \tag{35}$$

4.1.4.2 Forward Drag Terms

Now that thrust is defined as a function of propeller speed and vehicle velocity, the body-centered surge drag components can be determined directly. This will often be the drag term of greatest magnitude, since surge velocity will typically be much greater than other velocities. Thrust is assumed to be equal to drag once the vehicle has

accelerated to a steady-state velocity, thus allowing a nonlinear function for surge drag of

surge velocity to be formed:

$$T_{ss} = X_{|u|u}|u|u + X_u u \equiv D_{11}(v) \tag{36}$$

Using at least three data points for thrust as a function of velocity (including *T(0)*

= 0), it is possible to fit a second degree polynomial in the form of (36). It may be that a

linear model for drag is more accurate, reducing to:

$$D_{11}(v) = X_u u \tag{37}$$

4.1.4.3   Other drag terms and added mass

Sway and yaw drag terms cannot be found directly because it is not possible to

force the vehicle to travel in a purely sway or yaw direction. However, it is possible to

start from previously published works containing drag terms [20] [22] [39] as well as

guidelines for added mass terms [2] and tune these values using open loop simulation.

This refers to a simulation in which inputs are given for port and starboard propeller

speeds with an output of trajectory, velocity and heading which can be compared to

experimental results, as mentioned above. The dynamic model in (17) is used in this

process, rearranging to find body-fixed acceleration as a function of thrust vector (38),

then integrating to find velocity and integrating again to find position, which is

transformed to earth-fixed coordinates. A Simulink model for this purpose is seen in

Figure 4-2, designed for model constants to be tuned from a Matlab script which also

reads motor speeds used in experiments from an Excel spreadsheet.

$$\frac{[\tau_{control} + \tau_{env} - C(v)v - D(v)v]}{M} = \dot{v} \tag{38}$$
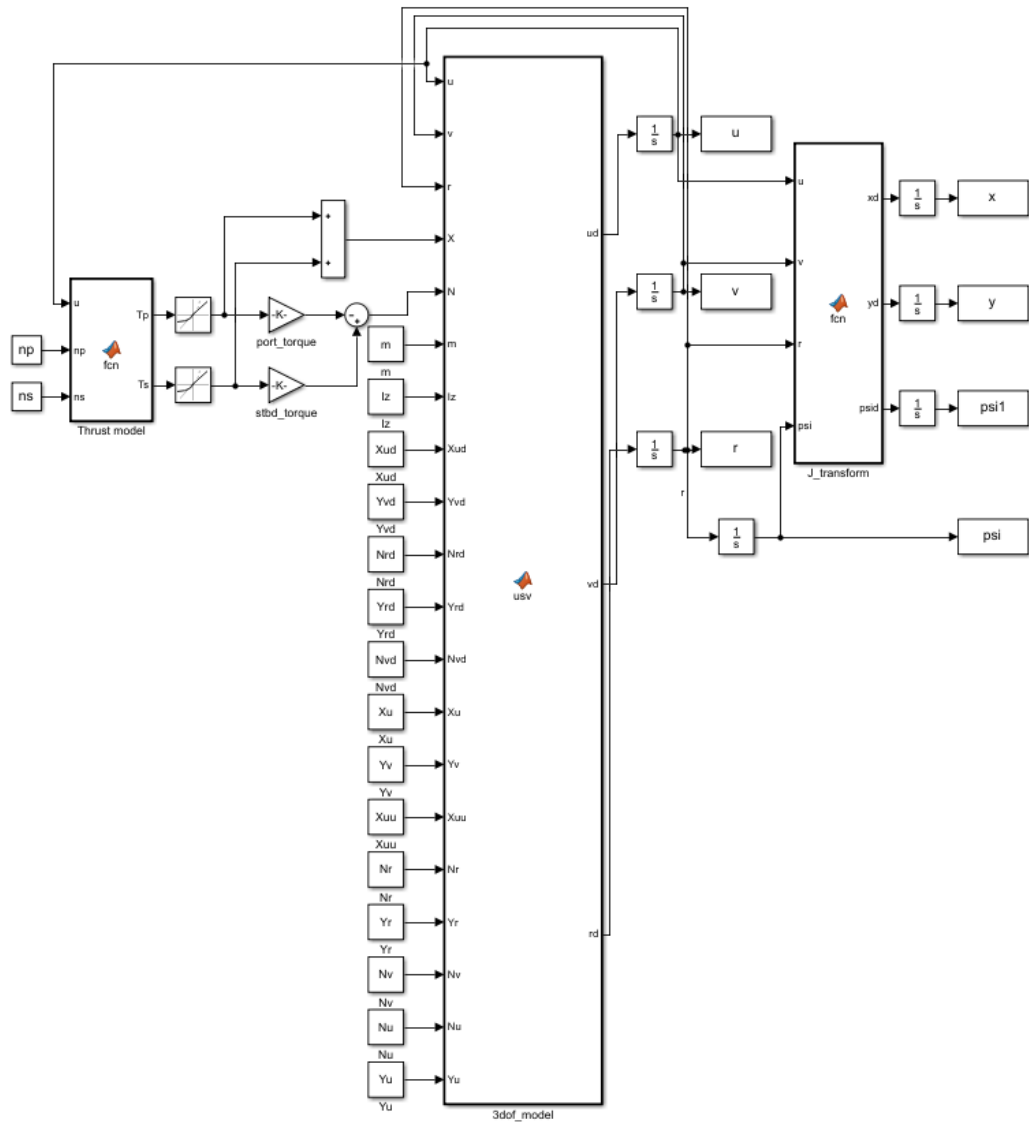
Figure 4-2: Open loop simulation model in Simulink

4.2   Controller Design and Simulation

The controller design in this thesis will attempt to address the problems of station-keeping and transiting between waypoints of an unmanned surface vehicle because of the usefulness of these functions as explained in the introduction. Station-keeping is the function of using control elements to maintain the vehicle in a fixed location while the transiting function explored here will attempt to follow a series of discrete trajectories between a series of user defined waypoints.

This section will describe the design of the feedback controller, the waypoint following function, the nonlinear observer, the control allocation to convert the control force from the controller to the force experienced by the vehicle given the constraints of equipment, the creation of synthetic vehicle motion data and the introduction of environmental disturbances.

4.2.1   Feedback Controller

4.2.1.1   Station-keeping

For station keeping, the simulation has been developed with a multi-input, multi-output (MIMO) PID controller which applies gains and the coordinate transform to output a force vector from a state error input. The control law is given as:

$$\tau_1 = -K_P J(\eta)^T \eta_t - K_D [J(\dot{\eta})^T \eta_t + J(\eta)^T \dot{\eta}_t] - K_I J(\eta)^T \int \eta_t \, dt \qquad (39)$$

$$K_P \equiv Proportional\ gain, K_D \equiv Derivative\ gain, K_I \equiv Integral\ gain,$$

$$\eta_t \equiv Earth\ fixed\ position\ error$$

The integral term will be set to zero in this design. It was previously observed [39] that the integral term in this style of controller would cause poor performance in station keeping due to an inability of the controller to produce required forces in the vehicle

sway direction and it was observed during preliminary controller design that even a small

integral term tended to cause instability.
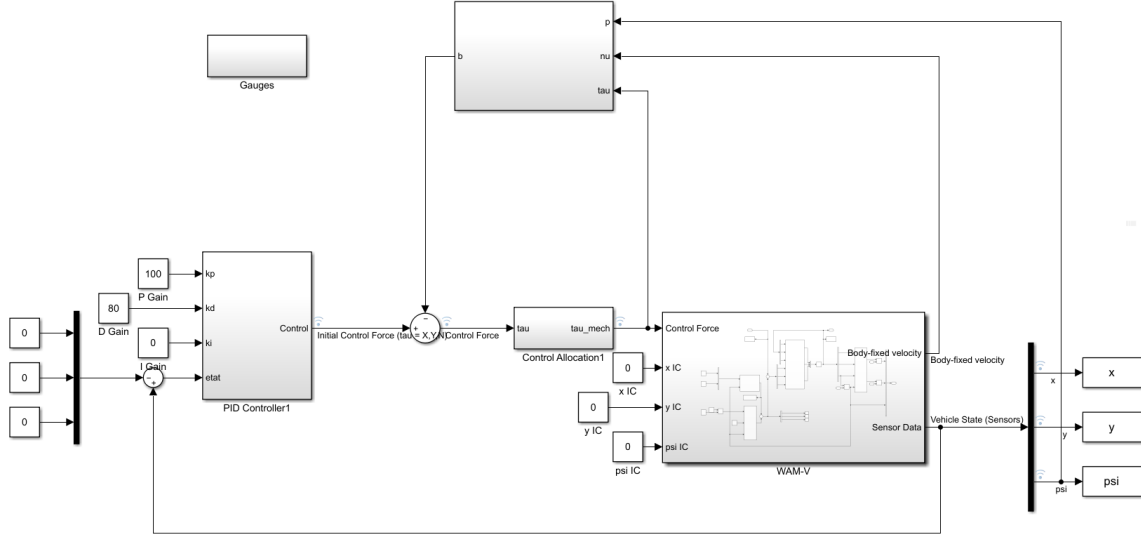
Figure 4-3: Station-keeping control system

4.2.1.2   Transiting

The transiting controller is comprised of three Simulink PID controller blocks

corresponding to the state error in three degrees of freedom: the velocity error in the

surge direction, the cross-track error (CTE) from the desired trajectory for the sway

direction and the heading error from the next waypoint. The separate blocks allow for

faster simulation and for a different controller to be used for the surge velocity, if needed,

due to different dynamics from heading and cross-track error. When a derivative term is

used in this Simulink block, a filtering term, N, is also used to dampen the response to a

rapidly changing error signal. The transfer function is as follows [40]:

$$C(s) = P + D\left(\frac{Ns}{s+N}\right). \tag{40}$$

Heading and CTE are tuned at the same time, with the error signal of CTE scaled

down to prioritize heading control. As with the station-keeping control, gains are

generally tuned by increasing the P gain until the desired state is reached and then

increasing the D gain until oscillations are smoothed sufficiently, but the Simulink PID

tuner tool was also used. The transiting control system is shown in Figure 4-4 and the

controller subsystem for the transiting mode is shown in Figure 4-5. Low pass filtering is

introduced for error signals to reduce oscillation of control forces. A difference from the

station-keeping controller is that the rotation matrix is not needed for all three degrees of

freedom. A cosine function of the angle in difference from the straight line between

waypoints is introduced in the sway direction to ensure that this control force is

proportional to the correctness of its direction.

There is no attempt made to control surge speed precisely because this is usually

not needed. A constant surge force is fed forward in addition to the surge force

commanded by the feedback controller to allow the vehicle to reach higher speeds with

lower controller sensitivity.
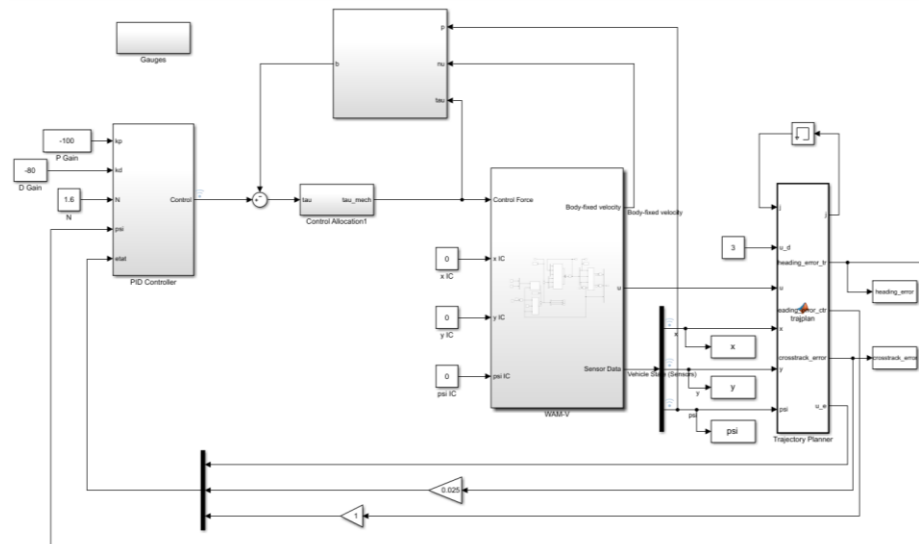
Figure 4-4: Transiting control system
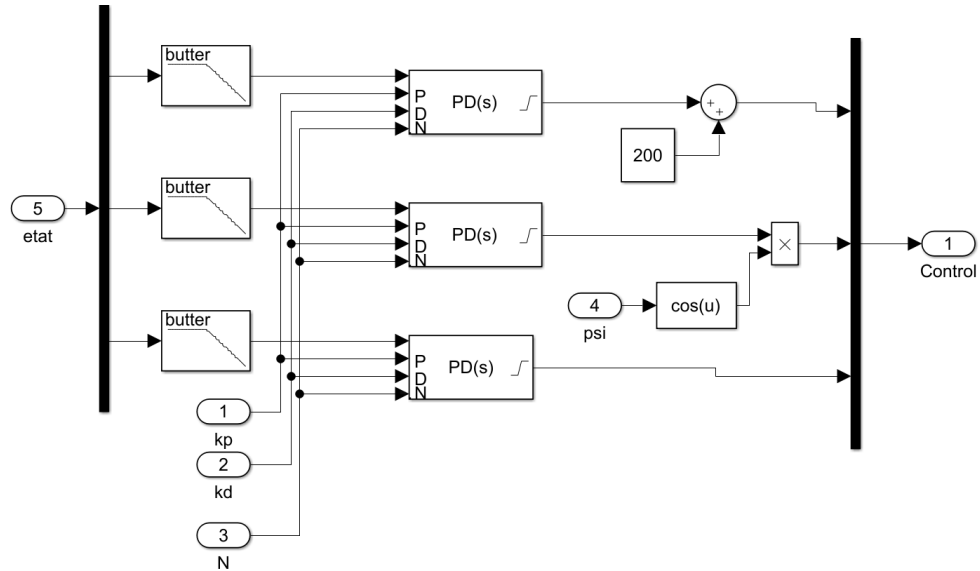
Figure 4-5: Transiting controller subsystem

4.2.1.2.1 Waypoint-following function

The transiting controller contains a function to construct a desired trajectory from waypoints and a reference speed and then output speed, heading and cross-track errors which are used by the feedback controller. For each segment between waypoints, the function calculates the distance travelled from the first waypoint and angle of error from the desired straight-line trajectory. The distance travelled along the desired line is found, then the CTE as the third leg of this triangle. The CTE may now be fed to the feedback controller and the distance travelled along the desired line is used to switch to the next target waypoint when it is reached. Figure 4-6 illustrates this function.
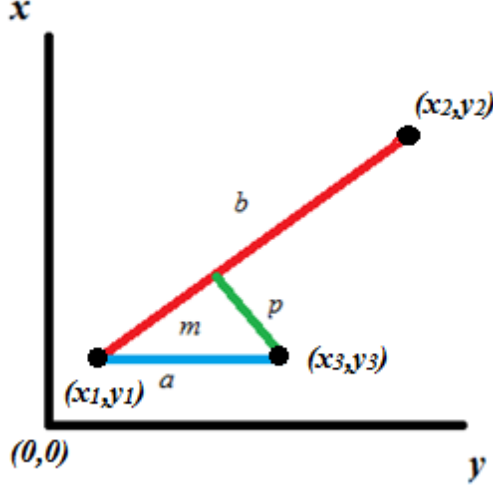
Figure 4-6: *(x₁,y₁)* shows the starting waypoint, *(x₂,y₂)* shows the destination waypoint, *(x₃,y₃)* shows the current vehicle position. *p* is the CTE and *m* is the distance travelled along the desired path.

4.2.2 Nonlinear Observer

The nonlinear observer from K. Do [17] described in the literature review section

is implemented to estimate the vector of unmodelled force acting on the vehicle. The

inputs to the observer are the force produced by the control elements (after control

allocation), the vehicle velocity vector and the vehicle heading. The equations describing

this observer from the literature review section are restated here:

$$\dot{x}_1 = F_1(x_1,\ x_2) \tag{6}$$

$$\dot{x}_2 = F_2(x_1, x_2, u) +\ G(x_1)d(t) \tag{7}$$

$$\hat{d}(t) =\ \xi + K_0 G^{-1}(x_1)x_2 \tag{8}$$

$$\dot{\xi} = -K_0\xi -\ K_0(\dot{G}^{-1}(x_1)x_2 + G^{-1}(x_1)F_2(x_1, x_2, u) + K_0 G^{-1}(x_1)x_2) \tag{9}$$

In this thesis, we will consider *x₁* to be earth-fixed position, *x₂* to be body-fixed

velocity and *d(t)* to be the earth-fixed disturbance force. Looking at equations (8-9), we

now only need to derive the function *F₂(x₁,x₂,u)* and *G(x₁)* using our knowledge of the

system.

32

$$x_1 = \eta = \begin{bmatrix} x \\ y \\ \psi \end{bmatrix}, x_2 = v = \begin{bmatrix} u \\ v \\ r \end{bmatrix} \tag{41}$$

$$\dot{x}_2 = \dot{v} = \frac{[\tau_{control} + \tau_{env} - C(v)v - D(v)v]}{M} \tag{42}$$

$$\frac{[\tau_{control} + \tau_{env} - C(v)v - D(v)v]}{M} = \frac{[\tau_{control} - C(v)v - D(v)v]}{M} + \frac{\tau_{env}}{M} \tag{43}$$

$$\tau_{env} = J^T(\psi)d(t) \tag{44}$$

$$\therefore F_2(x_1, x_2, u) = \frac{[\tau_{control} - C(v)v - D(v)v]}{M} \tag{45}$$

$$G(x_1) = \frac{J^T(\psi)}{M} \tag{46}$$

The remaining elements in the equations (8-9) are found by inverting $G(x_1)$, taking the time derivative of this inversion, and selecting a matrix K_0 from which the eigenvalues determine the aggressiveness of the observer in converging to the actual disturbance force. The dynamic term ξ is determined by solving for $\dot{\xi}$ and integrating the result, like how the acceleration of vehicle motion is determined and then integrated for velocity.

Do, himself, has a significantly more complex process for determining $F_2(x_1, x_2, u)$ and $G(x_1)$ because his controller is intended for a conventional, underactuated ship and thus he must find a way to respond to error in the sway direction when only able to control motion in the surge and yaw degrees of freedom [17]. I also found in simulations for transiting mode that feeding forward the sway term would cause major oscillations as the vehicle seemed to switch between correcting for yaw disturbance and correcting for sway disturbance. The solution was to add the sway disturbance force to the yaw disturbance force and feed this forward as the yaw disturbance. The control system is still fully actuated overall through the feedback controller. It was also found that for transiting the surge disturbance had no benefit for performance, so the signal was terminated.

33

Figure 4-7 shows the unmasked observer subsystem for station-keeping and Figure 4-8 shows this block for transiting, with surge force terminated and sway force added to yaw force.
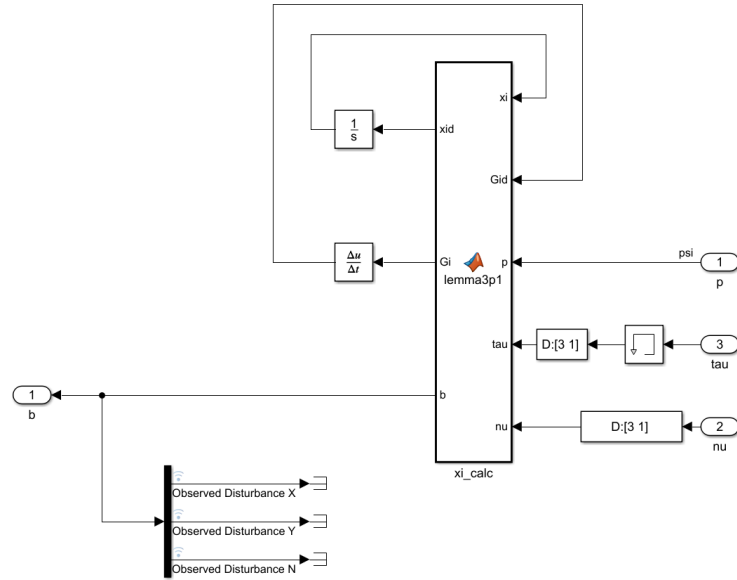
Figure 4-7: Observer block for station-keeping
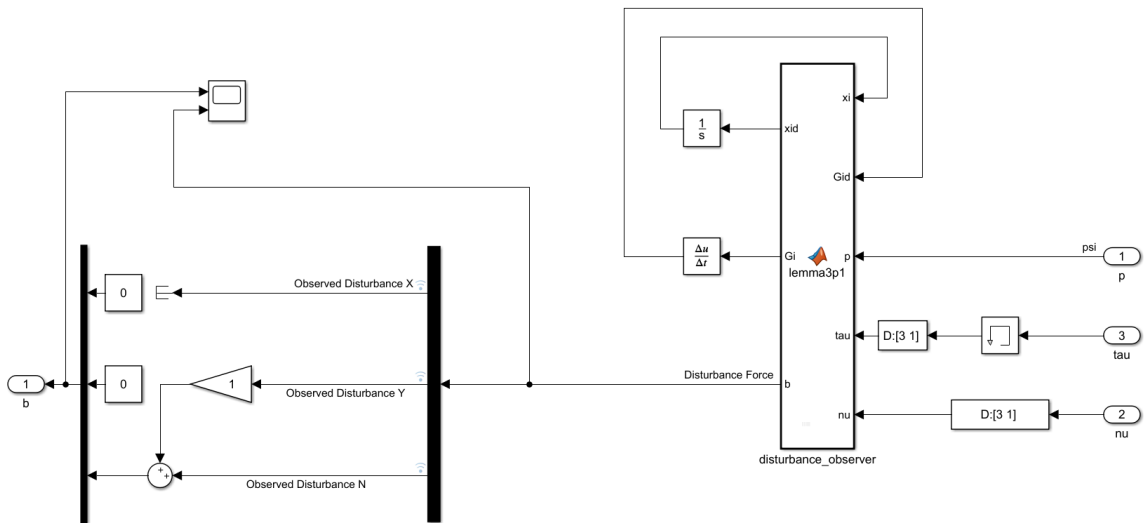
Figure 4-8: Observer block for transiting

4.2.3   Control Allocation

The control allocation problem is to create a process of determining actuator commands that will produce the thrust vector calculated by the controller. This process is complicated by constraints of thrust, angle and rate limitations imposed by actuator selection. The control allocation method developed for this simulation will thus have a thrust vector from the controller as an input and will output a thrust vector considering actuator constraints and vehicle geometry. As a fully-actuated system, there may be an infinite number of solutions to the thrust vector as a function of thruster force and angle and this process will choose one solution that fits within constraints.

The control allocation method used here will use the linear quadratic unconstrained using Lagrangian multipliers derived in [33]. An iterative process adapted from [36] is used where the thruster azimuth angle is low-pass filtered, rate limited and constrained to ±45° with a saturation function and then linear algebra is used to find thrust forces that will provide the desired thrust vector based on this angle. The rate limitation and saturation are based on the hardware constraints while the low-pass filter is used because the Lagrangian multiplier process can rapidly switch between different force and angle combinations. This algorithm improved results compared with using only saturation functions.

Thrust is expressed as follows:

$$\tau = Tf \tag{47}$$

$$T = \begin{bmatrix} 1 & 0 & 1 & 0 \\ 0 & 1 & 0 & 1 \\ -l_{y1} & l_{x1} & -l_{y2} & l_{x2} \end{bmatrix} \tag{48}$$

$l_{y1} \equiv Port\ thruster\ position\ from\ center\ of\ gravity\ along\ y-axis$

$l_{x1} \equiv Port\ thruster\ position\ from\ center\ of\ gravity\ along\ x-axis$

$$l_{y2} \equiv Starboard\ thruster\ position\ from\ center\ of\ gravity\ along\ y-axis$$

$$l_{x2} \equiv Starboad\ thruster\ position\ from\ center\ of\ gravity\ along\ x-axis$$

$$f = \begin{bmatrix} F_{x1} \\ F_{y1} \\ F_{x2} \\ F_{y2} \end{bmatrix}, Extended\ force\ vector \tag{49}$$

The extended force vector, f, represents forces in the x and y direction for the port and starboard thrusters. We now need to invert T in order to find f and allocate force to each thruster. If the thrusters equally weighted, this inverse reduces to:

$$T^{\dagger} = \mathrm{T}^{\mathrm{T}}(\mathrm{T}\mathrm{T}^{\mathrm{T}})^{-1} \tag{50}$$

So that:

$$f = T^{\dagger}\tau \tag{51}$$

From the extended force, individual thrust and azimuth angle components can easily be calculated:

$$T_{port} = \sqrt{F_{x1}^2 + F_{y1}^2}, T_{stbd} = \sqrt{F_{x2}^2 + F_{y2}^2} \tag{52}$$

$$\alpha_{port} = tan^{-1}\left(\frac{F_{y1}}{F_{x1}}\right), \alpha_{stbd} = tan^{-1}\left(\frac{F_{y2}}{F_{x2}}\right) \tag{53}$$

The control allocation function will now reverse the sign of thrust and rotate the angle by 180° if it is greater than ±90° for each thruster. Azimuth angles will now be fed through the rate limiter, saturation, and low-pass filter blocks and back into the function where thrust values (if the angle has changed) will be generated using linear algebra, now that the system is fully constrained.

The thrust signals are now fed through a saturation and rate limiting blocks and then converted back to a body-centered thrust vector. The control allocation subsystem is shown in Figure 4-9.
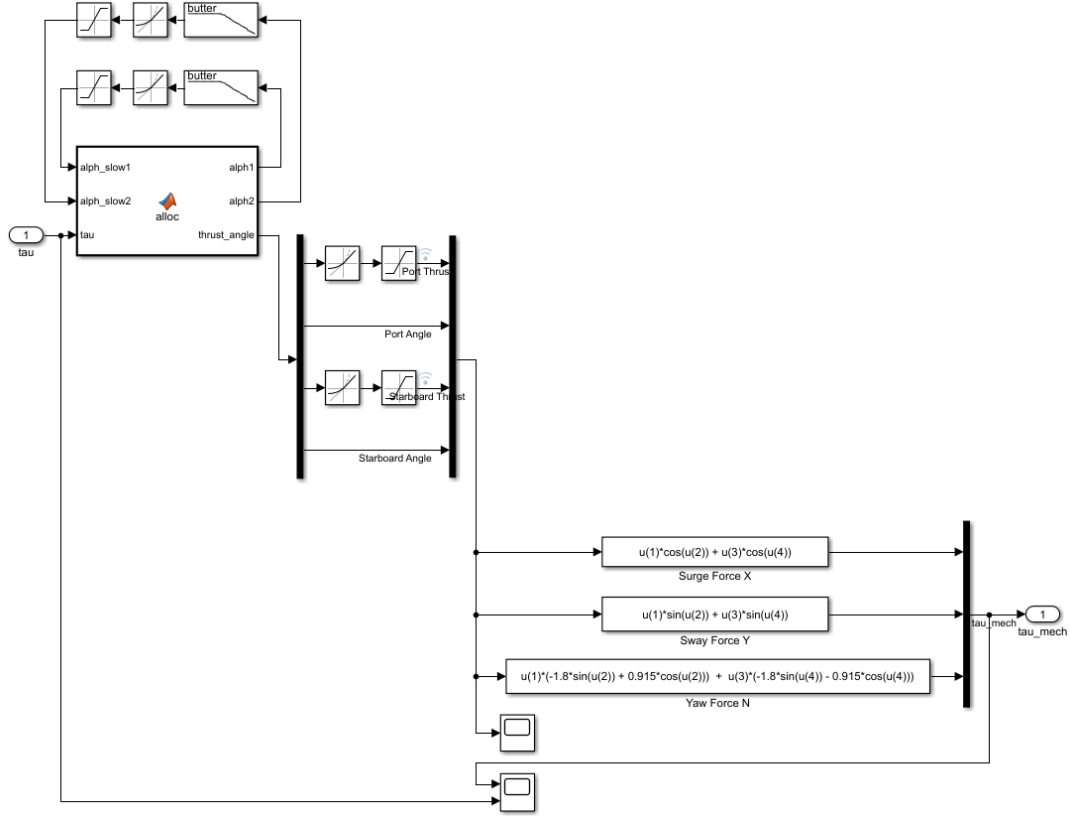
Figure 4-9: Control allocation subsystem

This process solves the control allocation problem to an acceptable point for this project. An alternative solution would be to develop an optimization algorithm that considers total energy usage and wear on actuators, but this may be too computationally demanding for a real-time microcontroller.

4.2.4   Simulated vehicle with environmental disturbances

The vehicle motion is simulated using the same process as in the open-loop simulation, with force inputs from the three degree of freedom force vector from the control allocation system, earth-fixed wind force and earth-fixed wave and current force.

The wave and current force is approximated by modeling the current speed as a velocity vector in the dynamic model, with acceleration assumed to be zero:

$$C(v_{wave\_current})v_{wave\_current} + D(v_{wave\_current}) = \tau_{wave\_current} \qquad (54)$$

The wave and current velocities are separated into north and east components and modeled using sin wave blocks so that a steady current can be modelled by setting the bias to the current speed and the amplitude to zero. A crude approximation of waves can be introduced by increasing the sin wave amplitude.

Wind is modelled using a technique shown in Fossen and by Qu et al. in [8] and [9]. Vehicle heading is compared to wind heading for an apparent angle of attack and wind force is calculated using the fluid drag formula.

$$\gamma_{apparent} = \psi_{wind} - \psi_{vehicle}$$

$$q = \frac{1}{2}\rho_{air}V^2$$

$$C_x = -c_x * cos(\gamma);$$

$$C_y = c_y * sin(\gamma);$$

$$C_z = c_z * sin(2\gamma);$$

$$\tau_w = q * [C_x * AF; C_y * AL; C_z * AL * LAA] \tag{55}$$

$$AF \equiv Frontal\ Area, AL \equiv Lateral\ Area, LAA \equiv Vehicle\ Length$$

$$c_x, c_y, c_z \equiv coefficients\ for\ force\ in\ surge, sway\ and\ yaw$$

In this simulation, wind gusts are modelled using the product of a pulse wave and a sine wave for a smoothly changing wind velocity that also introduces a discontinuous disturbance to the system.

Air density is calculated using air pressure, temperature and the ideal gas constant for air. The force coefficients are taken from Sarda et. al. [39] and the frontal and longitudinal areas are estimated using direct measurement. Table 4-1 shows constants used in the wind model and Figure 4-10 shows the WAM-V motion simulation.

Table 4-1: Wind model constants

Wind model constants	
ρ (kg/m^3)	1.19
c_x	0.50
c_y	0.50
c_z	0.33
AF (m^2)	0.71
AL (m^2)	1.49
LAA (m)	4.88
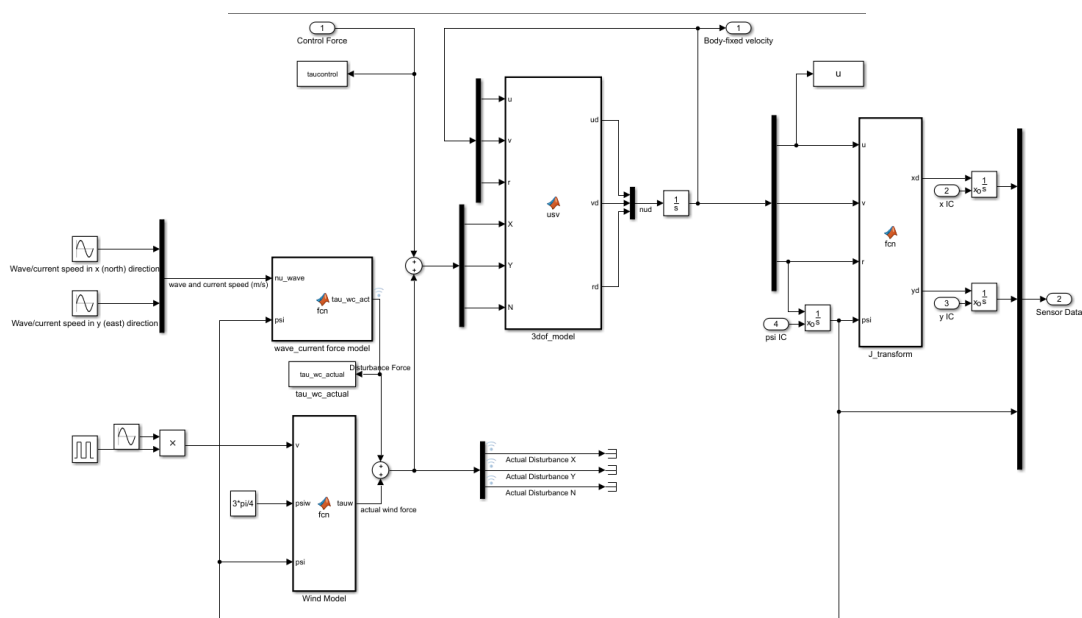
Figure 4-10: WAM-V motion simulation

4.3 Validation

Validation of the entire control system is required to prove adequate performance and specifically to prove the effectiveness of this type of disturbance observer, which has not been used previously with a fully actuated vehicle using a PD controller to my

knowledge. Adequate performance for this vehicle control system is defined as demonstrating the ability to remain at the target location (station-keeping) or track the desired trajectory (transiting) with minimum error and minimum excessive energy use. The validation portion of this thesis will be entirely in simulation and has two primary goals:

1. Run simulations of the control system and log data from various parameters and then subjectively determine whether these parameters are acceptable in the same way that the vehicle would be tested in "in real life" with engineers taking note of what they notice to be unacceptable deviations or abnormalities.

2. To validate the use of the disturbance observer specifically, simulate the vehicle without the observer as a "control sample" and then compare performance with simulation run with observer.

For both goals, the level of performance with regard to error will be evaluated by finding the variance of position and heading from the target position and heading:

$$\sigma^2 = \sum_{i=1}^{n} \frac{(x_{actual} - x_{desired})^2}{n} \tag{56}$$

For the station keeping case, variance will be taken of the absolute position error on the North-East coordinate plane in meters and the heading error in radians. For the transiting case, variance will be taken of cross-track error and heading.

Energy in a mechanical system is defined as force multiplied by displacement. While we will have data for the force used by our thrusters in the simulation and displacement, quantifying a comparison with a "perfect" controller is a complex question. A very simple way to approximate excessive energy use is to measure only the excessive

motion of the vehicle. For the station-keeping case, this will mean summing the total

movement of the vehicle between each discrete data point and dividing this by time for

the average absolute velocity of the vehicle (the target being zero). The same measure

can be done with the heading.

$$average\ linear\ velocity = \frac{\sum_{i=1}^{n-1} \sqrt{(x_{n+1}-x_1)^2-(y_{n+1}-y_1)^2}}{\sum time} \tag{57}$$

$$average\ angular\ velocity = \frac{\sum_{i=1}^{n-1} \psi_{n+1}-\psi_n}{\sum time} \tag{58}$$

For the transiting case, a percentage motion error will be found by summing the

absolute change in position between each discrete point, subtracting the displacement

along the target trajectory, and dividing by the displacement along the target trajectory.

$$\%_{error} = \frac{(\sum disc.displacements)-(length\ of\ target\ trajectory)}{(length\ of\ target\ trajectory)} * 100\% \tag{59}$$

This percentage error is taken of linear and angular displacement. For the angular

displacement, only one discrete point is used per second to avoid counting oscillations

lasting for less than one second.

The surge speed precision in transiting mode is not seen as important and the

controller is tuned for the surge speed to remain below the set point, but the total amount

of time to complete the waypoint mission is recorded to understand the effect of the

observer on surge speed.

4.3.1 Integral of the Square of Error for Performance Evaluation

The measures of error discussed above are straightforward but are not as

commonly used in control system design as the integral of the square of the error (ISE).

As shown below, ISE is the sum of the areas under a curve of error squared [41].

$$ISE = \int_0^T error^2(t)dt \tag{60}$$

ISE has an advantage of reaching a minimum value when the control system reaches a compromise between an overdamped (excessively slow) and underdamped (excessively aggressive), because both cases would cause errors which would increase ISE. Another advantage is that since there is no division by the number of discrete points, total time or trajectory, the ISE method may be used to compare control systems in tests with different end times, if the number and type of transients in the system is similar.

The variance, average velocity and percentage error measures described above will be sufficient for this thesis for comparing results with different variables because of consistencies in simulation time (for station keeping) and simulation target trajectory (for transiting), however for future work on this project ISE will be used to facilitate comparisons with other studies of USV control engineering.

5   Results

Results are presented here for the system identification testing and analysis

process, which includes two approaches to modeling thrust and the estimation of dynamic

model coefficients, as well as simulation parameters and results from station-keeping and

transiting simulations.

5.1   System identification

System identification results will include results of the bollard pull test to develop

the thrust model, results of the straight-line test relating speed to drag, and the calculation

of the surge drag terms, results relating the circle tests to propeller speed and figures of

open loop simulation results overlaid with experimental results. The final hydrodynamic

coefficients are seen in Table 5-4.

5.1.1   *Bollard pull test*

As described in the approach section, the process of thrust modelling began with a

bollard pull test. Only the maximum static thrust was recorded. The maximum static

thrust from our test and this value from Torqeedo's specifications are listed in Table 5-1.

The manufacturer specifications differ from our vehicle in the maximum propeller speed

achievable (due to restraints built into the GNC system), and consequently, in the

maximum static thrust achievable. This results in approximately 9% error in the static

thrust coefficient which could be explained by factors such as a difference in water depth

at our test site or difference in depth of the propeller below the water surface. The

nonlinear propeller thrust model described in the approach section is attractive to develop

a more realistic dynamic model. In the future it would be worth exploring the use of

Torqeedo's power monitoring features and using the published total efficiency from

electrical to propulsive force to generate a function of thrust as a function of propeller

speed and forward velocity, measuring thrust by mounting strain gauges on each thruster,

or conducting a dynamic thrust experiment using a tow tank with one thruster mounted

on the carriage moving a known speed and measuring the force generated by the thruster.

Table 5-1: Thruster constants, linear	Values for one thruster
Experimental max. static thrust	356 N
Manufacturer supplied max. static thrust	511 N
Experimental max. propeller speed for static thrust	1000 rev/min
Manufacturer supplied max. propeller speed for static thrust	1300 rev/min
Experimental static thrust coefficient $A = \frac{T_{max}}{n_{max}}$	0.356
Manufacturer supplied static thrust coefficient $A = \frac{T_{max}}{n_{max}}$	0.393

5.1.2 Straight-line test

The result shown in Table 5-2 display propeller speed (with both propellers

operating simultaneously), steady state surge speed and thrust according to the results

above. The result at full throttle (1000 RPM) is a significant outlier, and it is possible that

the propeller speed could have been lower than 1000 during that test because of the

electronic safety system which can limit current to the motor: Torqeedo lists its

maximum propulsive power as 1120 W per thruster, which would limit each thruster to

198 N at 5.65 m/s. With only four data points, if this data point were included it would

severely change the results so it was decided to leave it out. It was found that a linear

44

function for surge drag using the first three data points was the most accurate in comparing experimental data with open loop simulation.

Table 5-2: Straight-line test

Propeller speed [RPM]	Modelled thrust = drag [N]	Steady-state surge speed [m/s]
0	0	0
334	238	2.35
666	474	5.45
1000	712	5.65
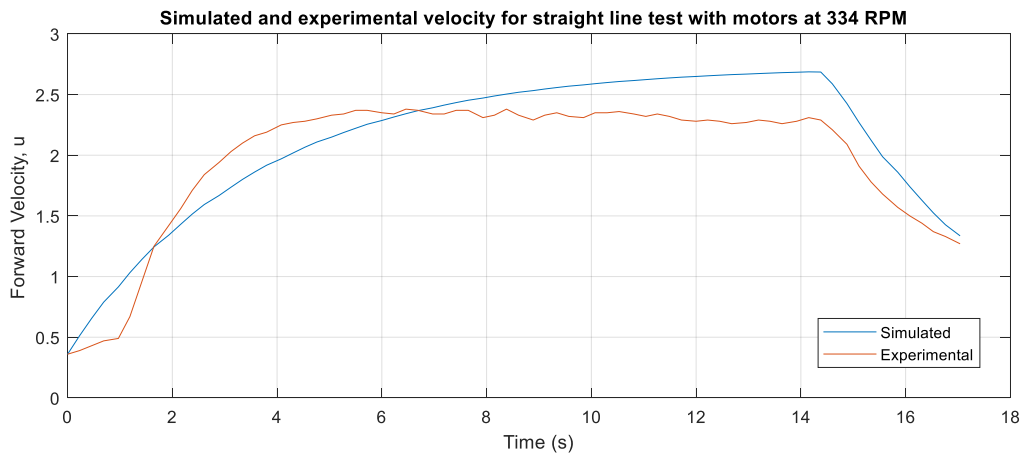
Figure 5-1: Straight line test at 334 RPM, speed vs. time
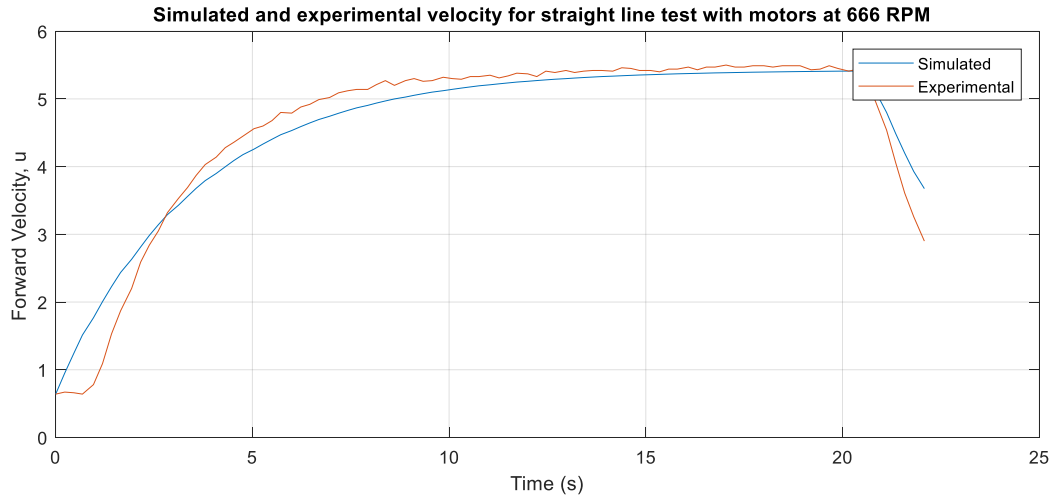
Figure 5-2: Straight line test at 666 RPM, speed vs. time

5.1.3   Circle tests

Circle tests measure the response of the vehicle to yaw force and are most useful for tuning drag terms that relate to yaw: N_r, Y_r and N_v. Circle tests were conducted in "large" form where only one thruster was activated and "tight" form where both thrusters were engaged in opposite directions. Table 5-3 shows the results of the circle test in steady-state yaw speed and Figure 5-3 shows one overlay of experimental and simulated results.

Table 5-3: Circle test results

Port RPM, Starboard RPM	Yaw force [N*m]	Steady-state angular velocity [rad/s]
0, 556	181	0.175
0, 778	253	0.170
0, 1000	326	0.154
-778, 778	506	0.488
-1000, 1000	652	0.479

46
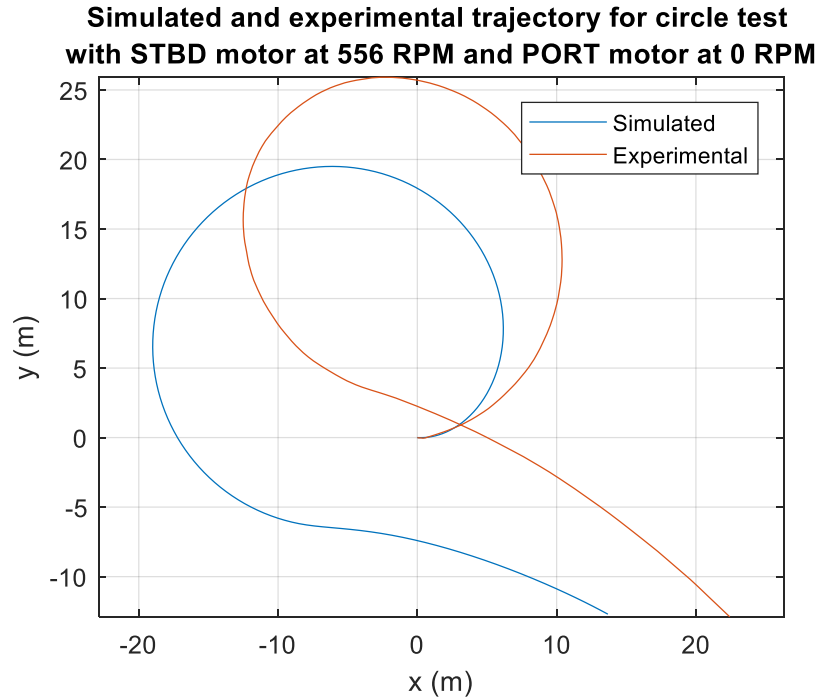
Figure 5-3: Large radius circle test

5.1.4 Zig-zag test

The zig-zag test is useful in tuning the remaining coefficients, including added mass, to match open loop simulation with experimental results. Zig-zag tests were performed at different propeller speeds with a consistent rate of alternation between thrusters. Figure 5-4 shows two zig-zag tests with experimental and simulated results of angular velocity over time. Note that the experimental angular velocity appears more uneven than the experimental surge velocity from the straight line tests because it is calculated using the discrete difference of heading over time while the surge velocity is supplied and filtered by the PixHawk.
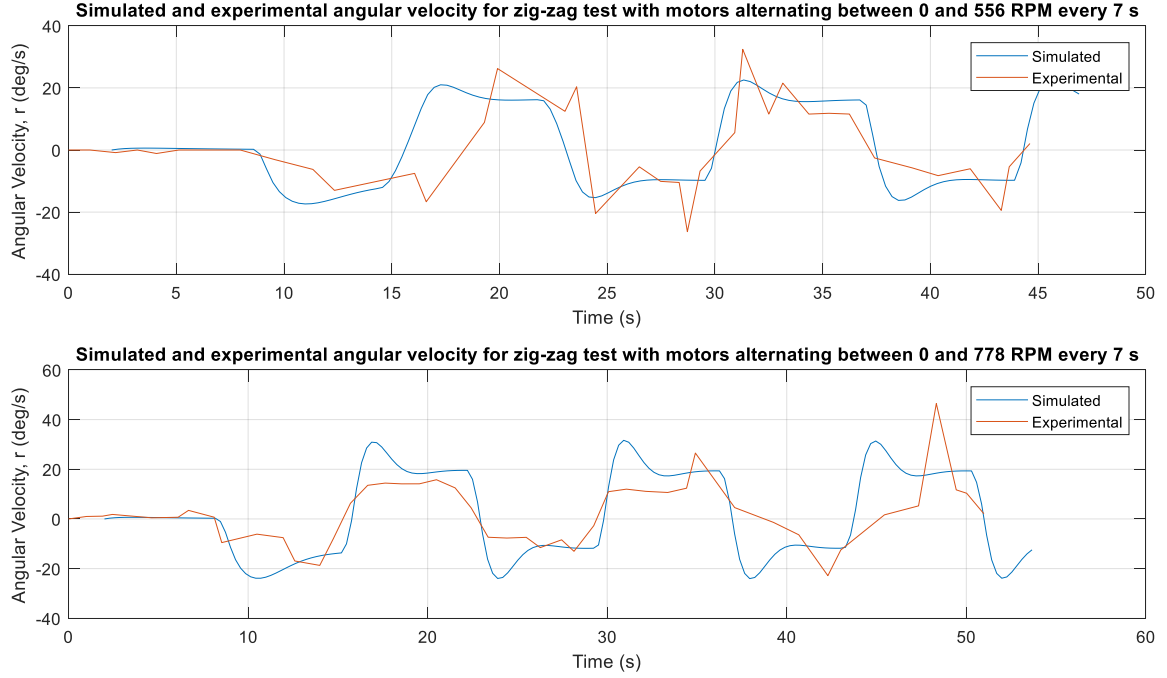
Figure 5-4: Zig-zag test results for angular velocity over time

5.1.5 *Final dynamic model constants*

While the surge dynamics are typically decoupled from other degrees of freedom, as mentioned above, it was found during system identification trials that our vehicle pulled heavily to starboard, justifying the insertion of the N_u drag coefficient into the dynamic model to be able to accurately tune the other coefficients. This coefficient will be left out of the controller simulation process and it is hoped that this problem would be corrected before this controller is used on the vehicle. The final dynamic model constants are shown in Table 5-4.

Table 5-4: Dynamic Motion model constants

Mass, m	280 kg
Moment of inertia, I_{zz}	300 kg $*$ m^2
Beam (center to center of hulls)	1.83 m
X_u	86.45 kg/s
$X_{\lvert u \rvert u}$	0
Y_v	300 kg/s
N_r	500 kg/s
N_v	-250 kg/s
Y_r	-80 kg/s
N_u	20 kg/s
$X_{\dot{u}}$	-30 kg
$Y_{\dot{v}}$	-40 kg
$N_{\dot{r}}$	-90 kg
$N_{\dot{v}}$	-50 kg
$Y_{\dot{r}}$	-50 kg

5.2 Station-keeping

A total of eight simulations were conducted for the station-keeping mode. These corresponded to two directions of steady current (head-on to the vehicle and directly from the side), with two current speeds for each direction. For each combination of current speed and direction, the simulation was run with and without the observer enabled. There was one wing gust occurring halfway through the simulation. Water current speed and wind gust speed were chosen to represent typical values. Consistent simulation parameters are shown in Table 5-5.

Results are shown in Table 5-6. Figure 5-7 shows these results plotted with current on the x-axis, different styles of line for different error measurements and with the use or absence of the observer indicated by color. From this figure we see that the observer does not have a major impact on average linear velocity and average angular velocity. The observer seems to increase these measures slightly at certain current velocities, but we can see from the $\log_{(10)}$ scale of the y-axis that they stay within the same magnitude. Position and heading variance, by contrast, are an order of magnitude higher without the observer at every current velocity.

Figure 5-5 and Figure 5-6 show the behavior of the station-keeping control system in the case of 0.5 m/s current to the East. The system with the observer enabled allows the vehicle to quickly move back to its desired position while the system without the observer maintains steady state error. The simulated wind gust is seen at 150 seconds and effects the heading and position of the vehicle but does not cause instability.

These results validate the performance of the control system generally in station-keeping and specifically the use of the disturbance observer. The observer causes the

control system to station-keep more accurately without significant increase in excessive motion.

Table 5-5: Station-keeping simulation parameters

Initial Condition x, y, ψ	0, 0, 0
Fixed-step size	0.01 [s]
Simulation stop time	300 [s]
Solver	Auto
Controller Gains K_P, K_I, K_D	100, 0, 80
Azimuth angle lowpass filter Passband edge frequency	12 [rad/s]
Wind gust peak velocity	12 [m/s]
Wind gust time length	30 [s]
Wind gust start time	150 [s]
Observer gain matrix	diag(0.1, 0.1, 0.1)

Table 5-6: Station-keeping results

Current speed [m/s]	Current Direction	Observer	Position Variance [m^2]	Heading Variance [m^2]	Average Linear Velocity [m/s]	Average Angular Velocity [rad/s]
0.5	North	Enabled	0.00424	0.00580	0.00757	0.00581
0.5	North	Disabled	0.07011	0.01472	0.00908	0.00534
0.5	East	Enabled	0.04824	0.01663	0.02768	0.01316
0.5	East	Disabled	0.43868	0.40216	0.01050	0.00430
0.7	North	Enabled	0.01427	0.02102	0.01800	0.01279
0.7	North	Disabled	0.38514	0.28811	0.00745	0.00315
0.7	East	Enabled	0.13651	0.03209	0.04075	0.01587
0.7	East	Disabled	0.73392	0.64292	0.09151	0.02429

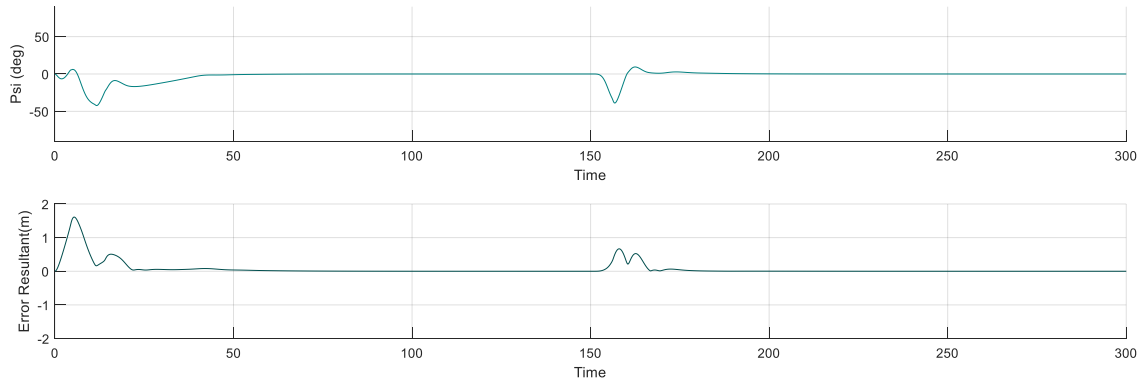Figure 5-5: Heading and position error from station keeping trial with current 0.5 m/s to the East with observer enabled
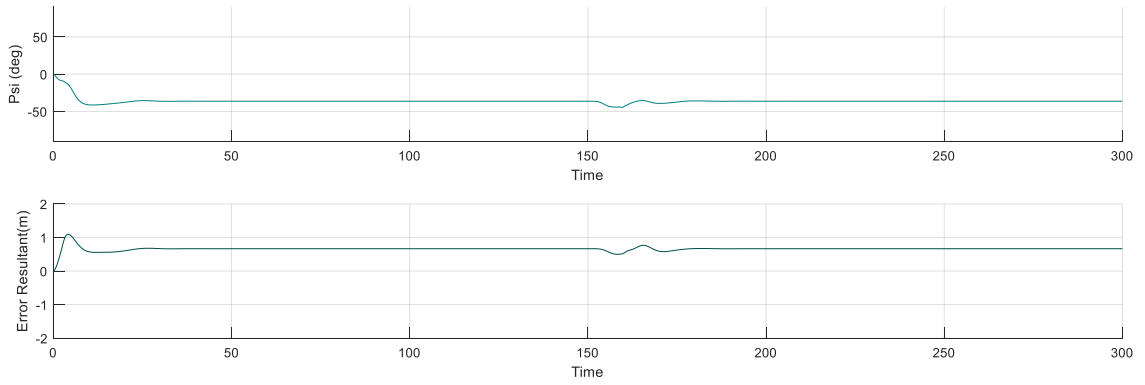

Figure 5-6: Heading and position error from station keeping trial with current 0.5 m/s to the East with observer disabled
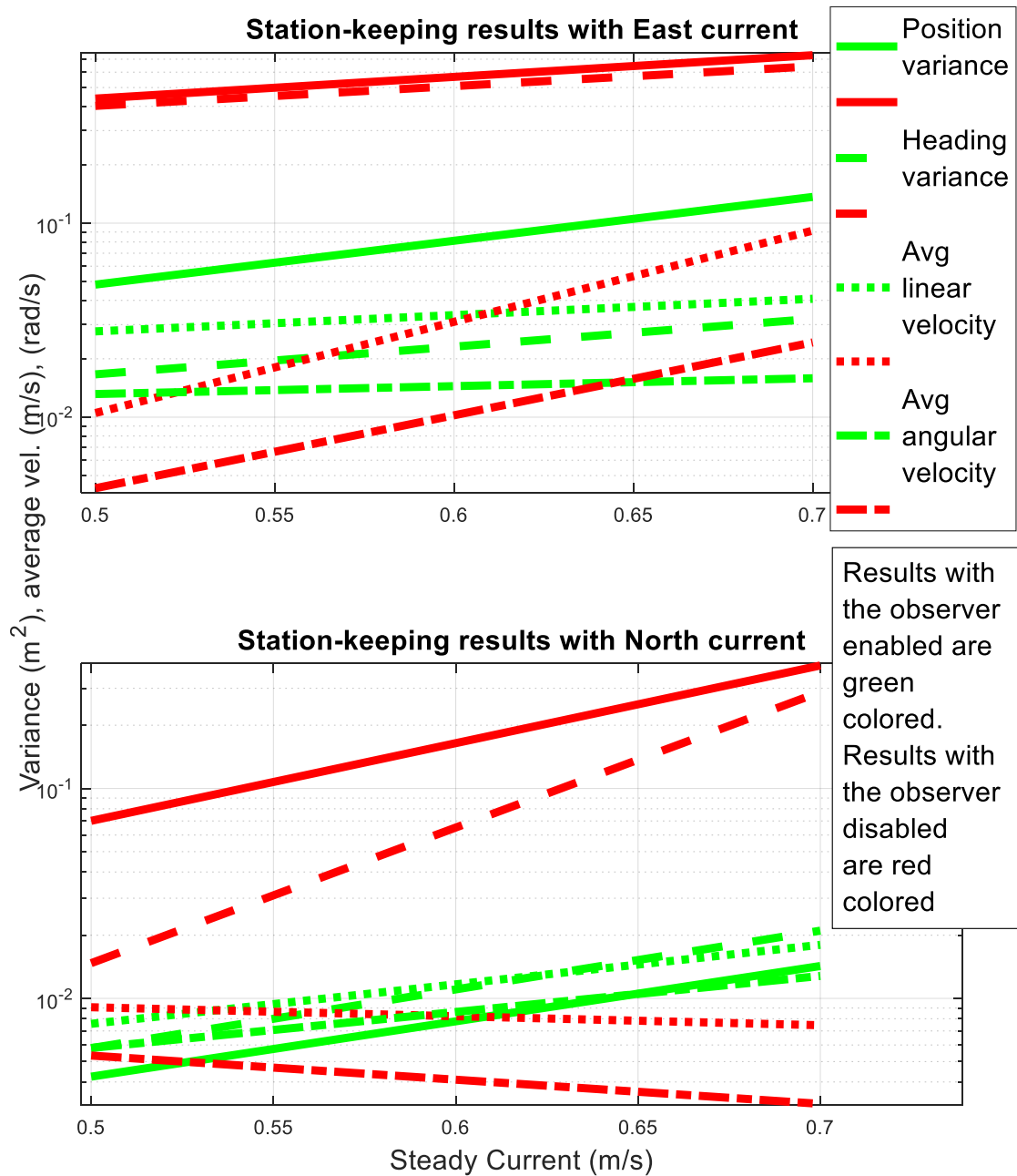
Figure 5-7: Results from station-keeping trials with eastward and northward current. Different line styles represent different measurements of error, plotted on the y-axis on a log(10) scale.

5.3 Transiting

Waypoint transiting will be simulated over a fixed desired path while current direction and speed will be changed, and the disturbance observer will be enabled and disabled in a similar pattern to the station-keeping trials. A simulated gust of wind will occur once roughly halfway through the simulation. The desired path is a lawnmower type pattern in which the vehicle will transit north for a fixed distance, turn 180 degrees in a semi-circle while moving east, transit south for the same distance and repeat this pattern. The desired trajectory is shown in Figure 5-8.
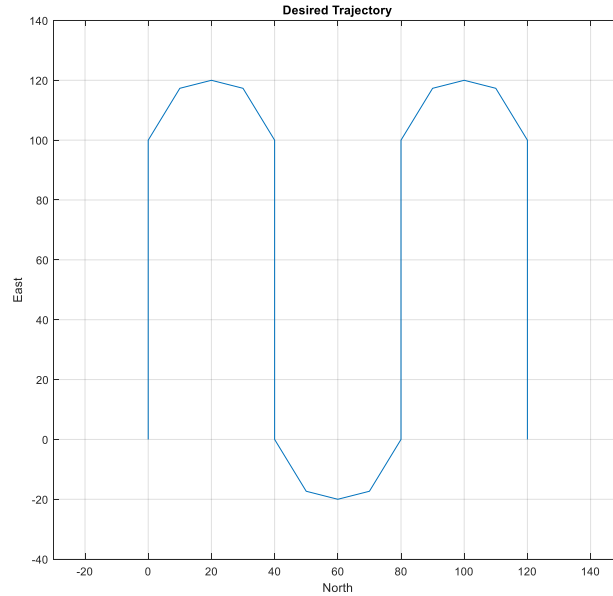

Figure 5-8: Transiting simulation target path

The results shown in Table 5-8, and graphed in Figure 5-9, Figure 5-10, Figure 5-11, and Figure 5-12 show satisfactory performance of the control system generally and an improvement in trajectory tracking when using the disturbance observer. There is not the same level of improvement as with the station-keeping controller, but in every

measure except for one (excessive angular displacement with current in the north direction) using the observer results in improved performance.

In Figure 5-9 and Figure 5-11, variance in CTE is much larger when current flows in the east direction because it is perpendicular to the intended path of the vehicle and this variance grows as current speed increases. The disturbance observer works most effectively here, reducing this variance to less than one fifth of its size at both current speeds. For visualization, Figure 5-13 and Figure 5-14 show the same current condition without and with the observer enabled, respectively, and there is a visible difference in the controller performance.

The effect on heading variance is much smaller and would be within reasonable limits with or without the observer. The percentage error in linear displacement shows us that using the observer results in less excessive linear motion in than without it, but the percentage error in angular displacement is contradictory in the northward current case, likely because the observer allowed the vehicle to be oriented closer to the same or opposite direction as the current.

The operation of the observer in the transiting control system, as explained in the Approach section, is to sum the sway disturbance force with the yaw disturbance and feed this forward, adding to the yaw force from the PD controller. This method is effective because of the negative sign of the N_v and Y_r terms: a disturbance force in the positive sway direction will generate a negative force in the yaw direction and vice versa. When exposed to steady current, the disturbance forces in these degrees of freedom will almost always be opposite of each other. Feeding forward each of these terms individually would produce instability that could only be corrected by the feedback

controller, but by summing them the degree of freedom experiencing the most disturbance force "wins out" and is able to influence the control force in the yaw direction to best reject that disturbance. For example, an observed disturbance force of negative 50 N in the yaw direction and positive 100 N in the sway direction would sum to positive 50 N, which would be fed forward as -50 N, turning the vehicle gently into the oncoming current to reduce its motion in the sway direction.

Table 5-7: Transiting simulation parameters

Initial Condition x, y, ψ	0, 0, 0
Desired surge speed, u	1.5 [m/s]
Fixed-step size	0.01 [s]
Simulation stop time	600 [s]
Solver	Auto
Gain for CTE error	0.025
Controller Gains K_P, K_I, K_D, N	100, 0, 80, 1.6
Bias added to surge force command	120 [N]
Azimuth angle lowpass filter Passband edge frequency	12 [rad/s]
Error to controller lowpass filter Passband edge frequency	12 [rad/s]
Wind gust peak velocity	12 [m/s]
Wind gust period	10 [s]
Wind gust start time	200 [s]
Desired trajectory length	588.5 [m]
Observer gain matrix	diag(0.1, 0.1, 0.1)

Table 5-8: Transiting results

| Current speed [m/s]	Current Direction	Observer	Cross-track error Variance [m²]	Heading Variance [m²]	Linear motion error [%]	Angular motion error [%]	Time to complete mission [s]
0.5	North	Enabled	3.829	0.03502	2.5519	20.206	428.6
0.5	North	Disabled	4.2522	0.03601	3.1261	16.009	431.0
0.5	East	Enabled	8.3744	0.14457	1.4654	60.894	402.4
0.5	East	Disabled	46.128	0.14672	4.4172	75.642	415.8
0.7	North	Enabled	5.4983	0.05012	3.2316	32.119	440.8
0.7	North	Disabled	6.417	0.05220	4.2578	20.473	445.6
0.7	East	Enabled	15.113	0.2278	0.25012	78.873	393.0
0.7	East	Disabled	87.413	0.2365	5.4441	88.713	417.4
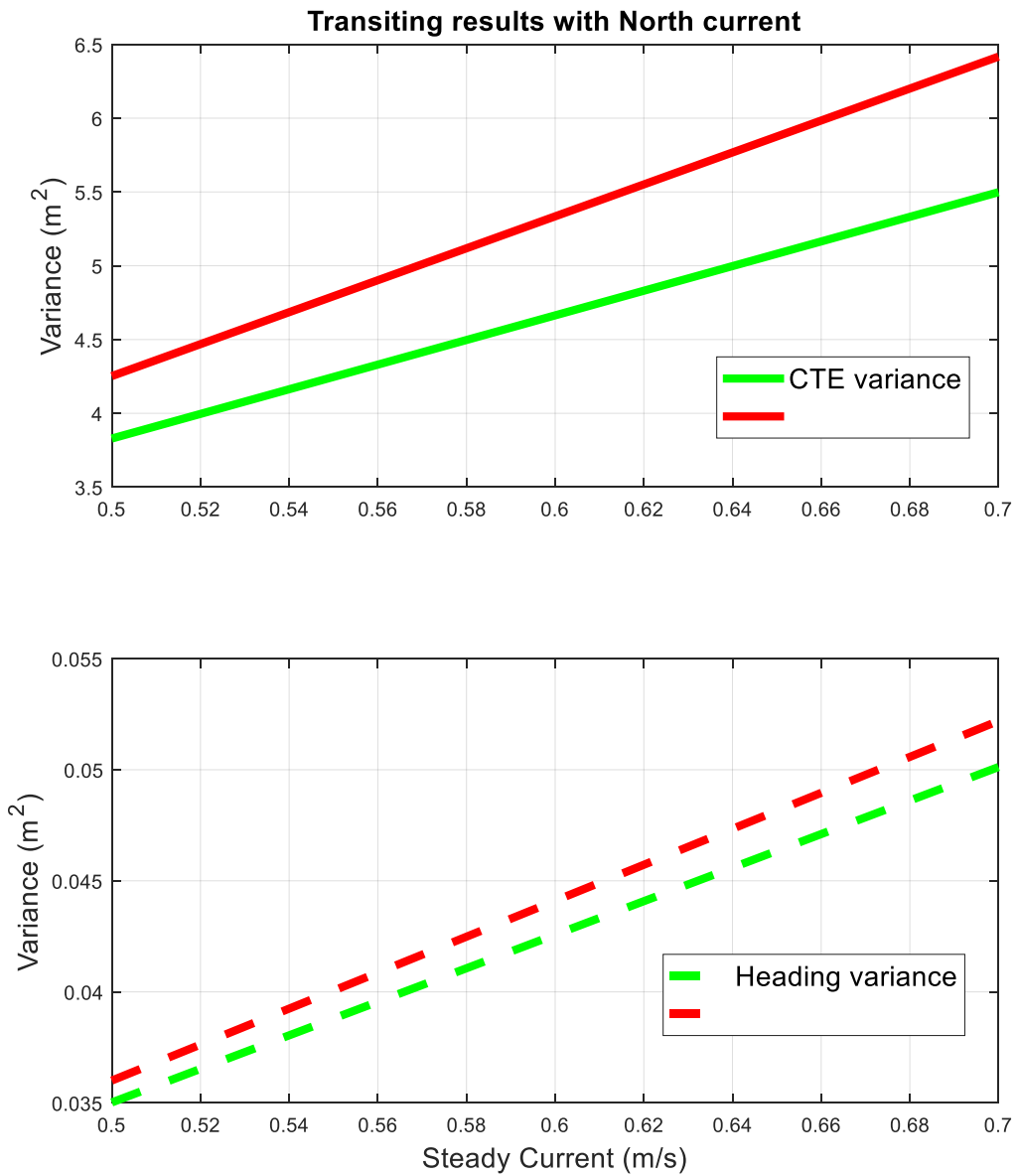
Figure 5-9: Transiting results with North current for variance. Green lines represent results using the observer while red lines represent results without using observer.
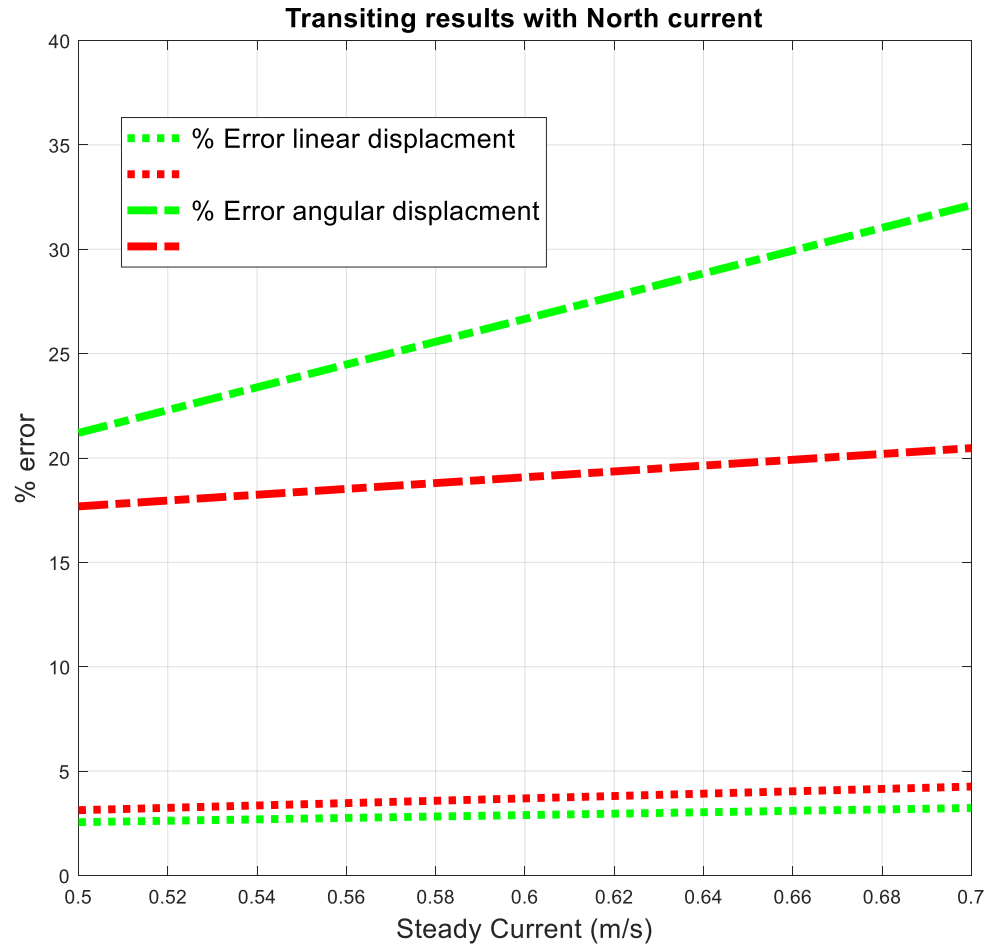
Figure 5-10: Results for percentage displacement error for transiting with current in the north direction. Green lines represent results using the observer while red lines represent results without using observer.

Figure 5-11: Results for variance with current in the East direction. Green lines represent results using the observer while red lines represent results without using observer.

Figure 5-12: Results for percentage displacement error with current to the East direction. Green lines represent results using the observer while red lines represent results without using observer.

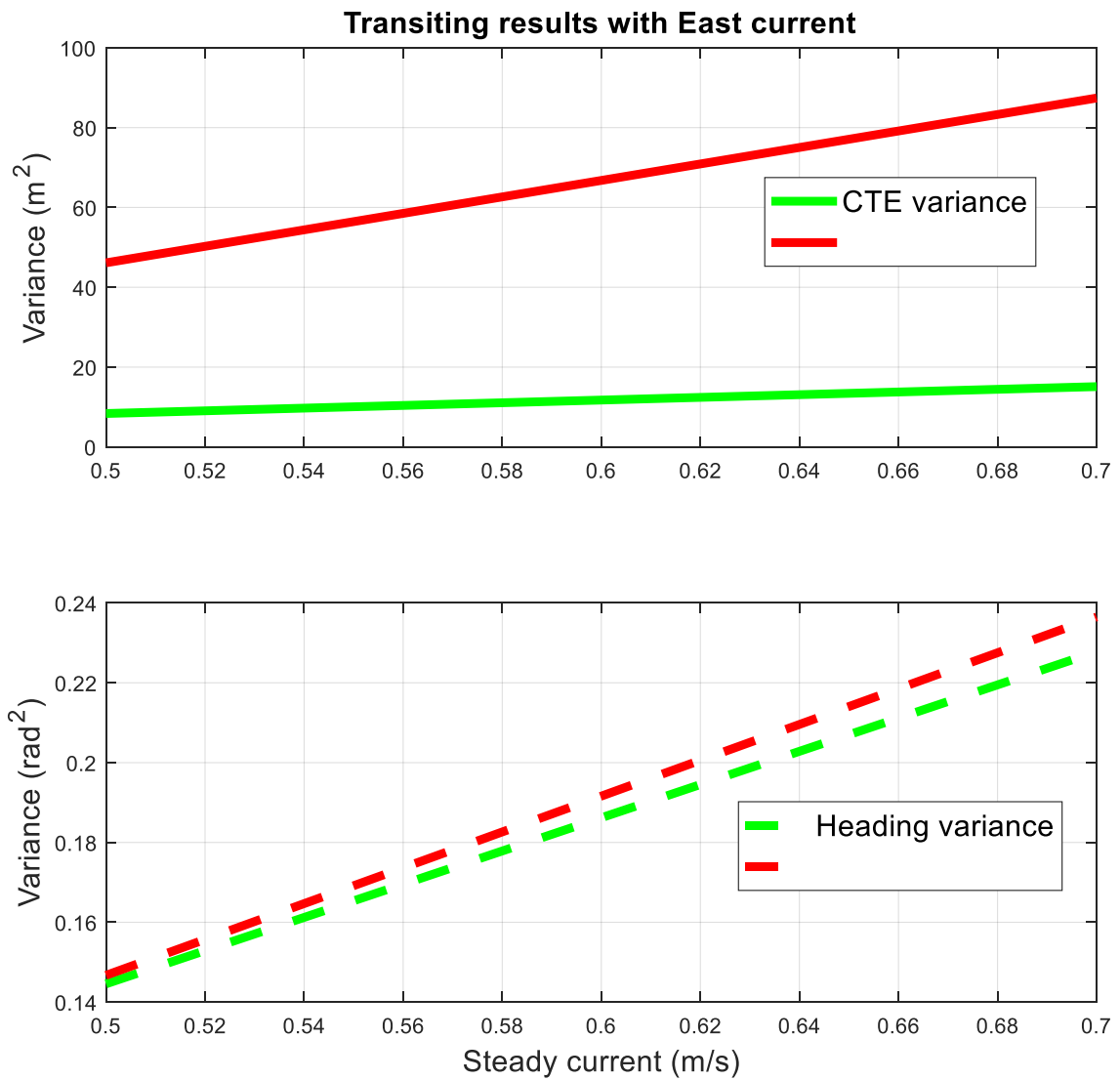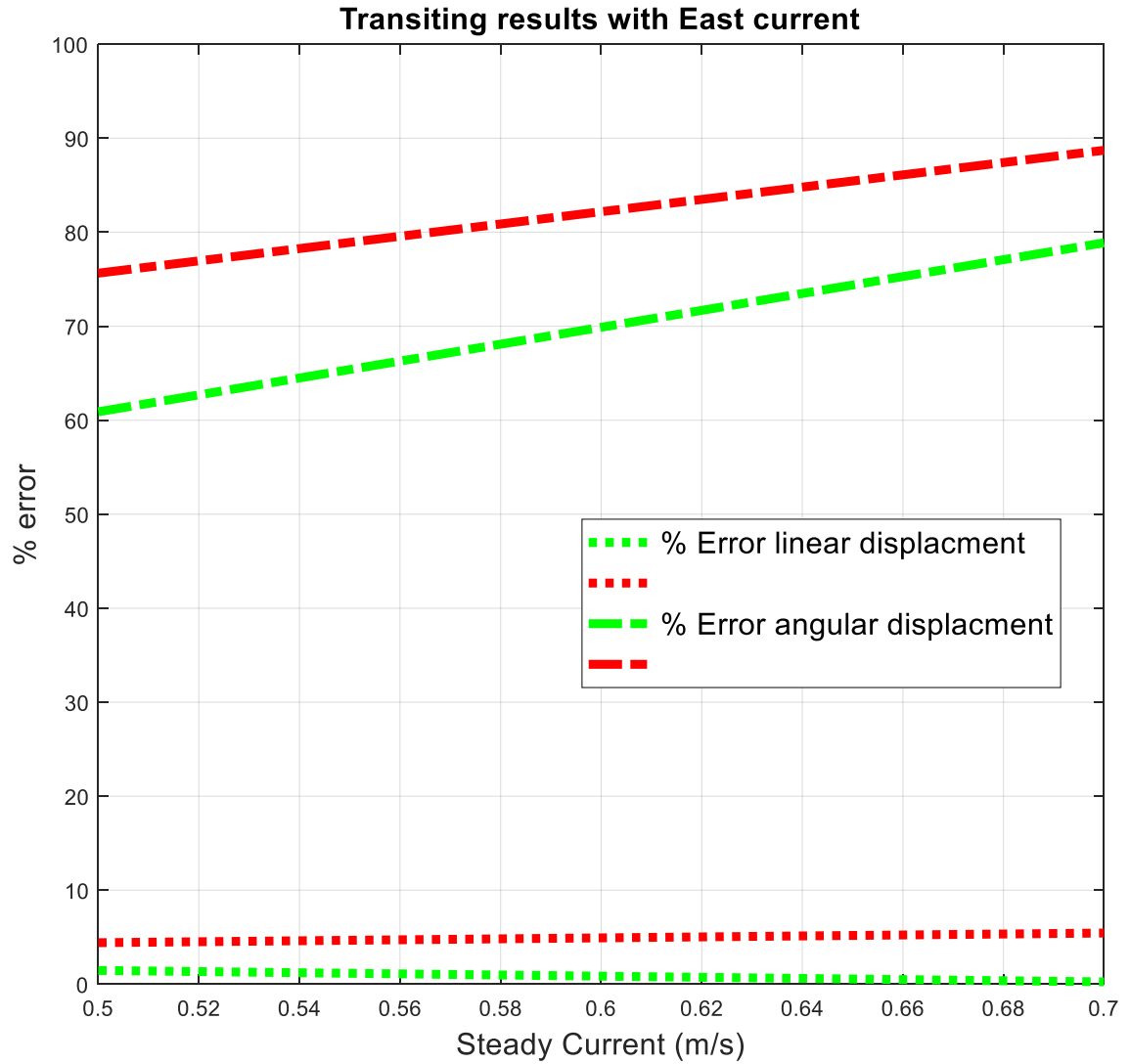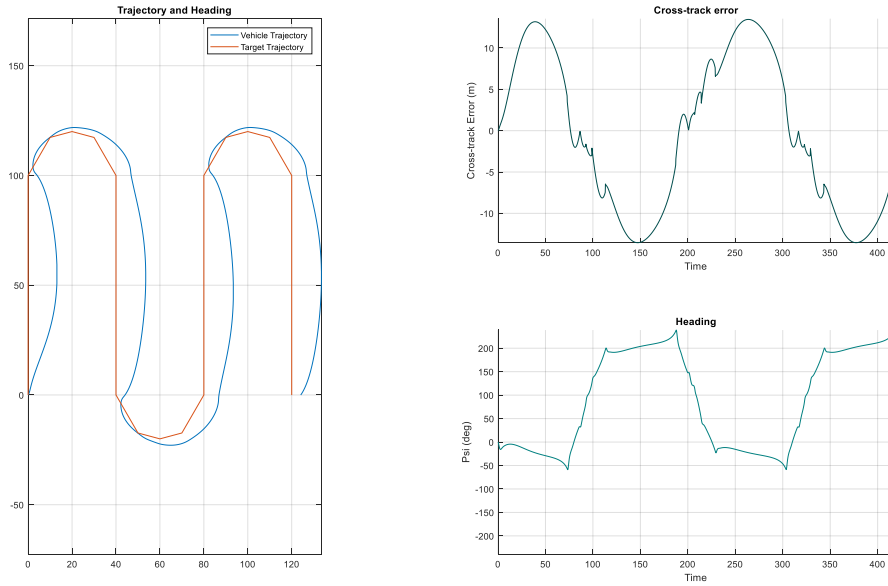Figure 5-13: Transiting trajectory, crosstrack error and heading with 0.7 m/s current to the East without observer
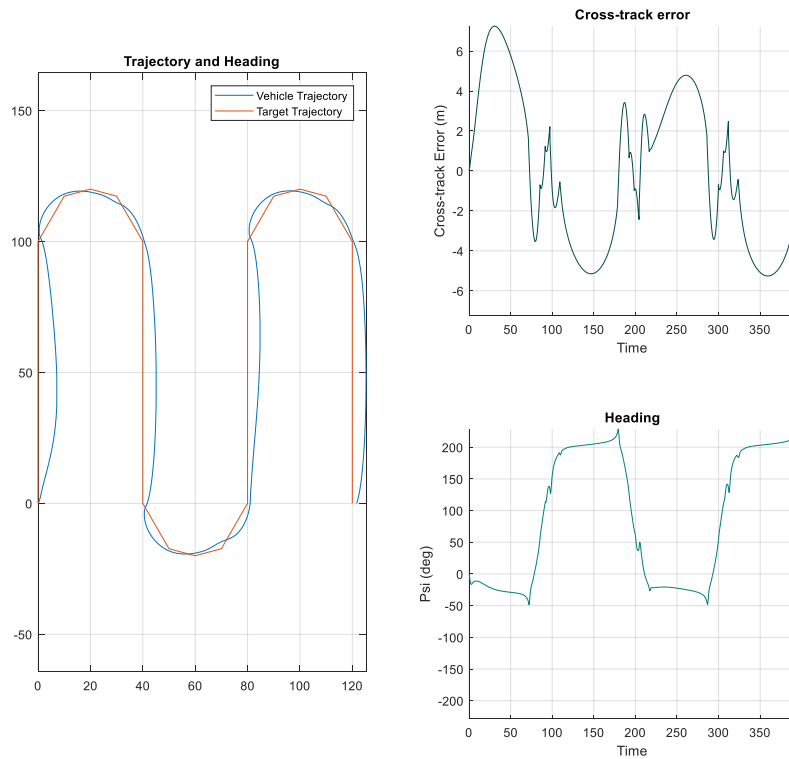

Figure 5-14: Transiting trajectory, crosstrack error and heading with 0.7 m/s current to East with observer

6   Conclusions

This thesis serves to apply known concepts to an existing platform in a novel way: a nonlinear observer is used in composite with a linear PD controller, a control allocation method is adapted to fit our equipment constraints and a waypoint following algorithm is created to measure crosstrack error to allow a fully actuated controller to be used effectively while transiting.

System identification is a crucial piece of implementing a controller in an actual system and a clear and detailed explanation of the process to find a dynamic model is given with contemplation on the necessity for accurate experimental modeling of thrust.

The benefit of the control system with the observer is demonstrated through testing the control system design and measuring the effect of the observer by running simulations with and without the observer activated. The results of these simulations show that the observer will always improve position accuracy in both station-keeping and transiting, with an occasional downside of increased energy use due to oscillation around the desired position or trajectory.

The integration of the observer into the system was not as straightforward as coding and tuning: the dynamics of our vehicle made feeding forward the disturbance force directly impossible and the sway force was added to the yaw force instead. This method of using a nonlinear observer is not common to my knowledge and deserves further study.

Adding this type of nonlinear observer to a control system has promising future potential: it could be combined with a weather station and current and wave measuring devices to measure wind, wave and current force which would provide faster and more accurate disturbance rejection. With a station-keeping vehicle and additional data post-processing, the disturbance observer could serve as an environmental monitoring station for measuring wind and current speeds and wave activity.

7 References

[1]   United States Navy, "The Navy Unmanned Surface Vehicle (USV) Master Plan," 2007.

[2]   T. I. Fossen, Guidance and Control of Ocean Vehicles, Chichester, England: John Wiley & Sons, Ltd, 1994.

[3]   Torqeedo GmbH, "Performance & Efficiency," [Online]. Available: https://www.torqeedo.com/us/en-us/technology-and-environment/performance-and-efficiency.html. [Accessed 5 March 2018].

[4]   "Power 26-104," Torqeedo GmbH, 2017. [Online]. Available: https://www.torqeedo.com/us/en-us/products/batteries/power-26-104/2103-00.html. [Accessed 10 December 2017].

[5]   B. Seiffert, Class Lecture, Topic: "Hydrodynamic Categorization of Marine Vehicles" EOC6515, Department of Ocean and Mechanical Engineering, Florida Atlantic University, Jan., 10, 2017.

[6]   A. Sinisterra, M. Dhanak and N. Kouvaras, "A USV platform for surface autonomy," in *OCEANS - Anchorage, 2017*, Anchorage, 2017.

[7]   Z. Liu, Y. Zhang, X. Yu and C. Yuan, "Unmanned surface vehicles: An overview of developments and challenges," Annual Reviews in Control, pp. 1-23, 2016.

[8]   H. Qu, E. Sarda, I. Bertaska and K. von Ellenrieder, "Wind feed-forward control of a USV," in *OCEANS 2015*, Genova, 2015.

[9]   H. Qu and K. D. Von Ellenrieder, "Adaptive wind feedforward control of an Unmanned Surface Vehicle for station keeping," in *OCEANS 2015 - MTS/IEEE*, Washington, D.C., 2015.

[10]   B. Messner, D. Tilbury, R. Hill and J. Taylor, "Control Tutorials for MATLAB and Simulink," 2011. [Online]. Available: http://ctms.engin.umich.edu/CTMS/index.php?example=Introduction&section =SystemModeling. [Accessed 9 3 2018].

[11]   G. Besançon, "An Overview on Observer Tools for Nonlinear Systems," in *Nonlinear Observers and Applications*, Berlin, Springer, 2007, pp. 1-31.

[12]   P. Beaujean, Lecture, Topic: "Position and Motion Sensing", OCE6625, Department of Ocean and Mechanical Engineering, Florida Atlantic University, 2017.

[13]   T. I. Fossen and J. P. Strand, "Passive nonlinear observer design for ships using Lyapunov methods: full-scale experiments with a supply vessel," *Automatica,* vol. 35, pp. 3-16, 1999.

[14]   W.-H. Chen, J. Yang, L. Guo and S. Li, "Disturbance-Observer-Based Control and Related Methods—An Overview," *IEEE Transactions on Industrial Electronics,* vol. 63, no. 2, pp. 1083 - 1095, 2015.

[15]   W.-H. Chen, D. Ballance, P. Gowthrop and J. O'Reilly, "A nonlinear disturbance observer for robotic manipulators," *IEEE Transactions on Industrial Electronics,* vol. 47, no. 4, pp. 932 - 938, 2000.

[16]   W.-H. Chen, "Disturbance observer based control for nonlinear systems," *IEEE/ASME Transactions on Mechatronics,* vol. 9, no. 4, pp. 706-710, 2004.

[17]   K. Do, "Practical control of underactuated ships," *Ocean Engineering,* vol. 37, no. 13, pp. 1111-1119, 2010.

[18]   H. K. Khalil, Nonlinear Systems, Upper Saddle River, NJ: Prentice Hall, 2002.

[19]   A. Sorensen, S. Sagatun and T. Fossen, "Design of a Dynamic Positioning System Using Model-Based Control," *Control Engineering Practice,* vol. 4, no. 3, pp. 359-368, 1996.

[20]   W. B. Klinger, I. R. Bertaska, K. D. von Ellenrieder and M. R. Dhanak, "Control of an Unmanned Surface Vehicle With Uncertain Displacement and Drag," *IEEE Journal of Oceanic Engineering,* vol. 42, no. 2, pp. 458-476, 2017.

[21]   T. I. Fossen and P. J. Strand, "Tutorial on nonlinear Backstepping: Application to Ship Control," *Modeling, Identification and Control,* vol. 20, no. 2, pp. 83-135, 1999.

[22]   E. Sarda, I. Bertaska, A. Qu and K. Von Ellenrieder, "Development of a USV station-keeping controller," in *OCEANS 2015*, Genova, 2015.

[23]   I. Bertaska and K. Von Ellenrieder, "Supervisory switching control of an unmanned surface vehicle," in *OCEANS'15 MTS/IEEE*, Washington, D.C., 2015.

[24]   J.-J. E. Slotine and W. Li, Applied Nonlinear Control, Englewood Cliffs, New Jersey: Prentice-Hall, 1991.

[25]   L. Desbourough and R. Miller, "Increasing customer value of industrial control performance -- Honeywell's experience," in *Sixth International Conference on Chemical Process Control. AIChE Symposium Series Number 326.*, 2002.

[26]   A. Karl Johan and M. Richard M., Feedback Systems, Princeton, New Jersey: Princeton University Press, 2008.

[27]   M. M. Hammad, "Trajectory following and stabilization control of fully actuated AUV using inverse kinematics and self-tuning fuzzy PID," *PLoS ONE ,* vol. 12, no. 7, 2017.

[28]   M. P. B. W. Yang Fang, "A course control system of unmanned surface vehicle (USV) using back-propagation neural network (BPNN) and artificial bee colony (ABC) algorithm," in *8th International Conference on Advances in Information Technology, IAIT2016*, Macau, China, 2016.

[29]   C. R. Sonnenburg and C. A. Woolsey, "Modeling, Identification, and Control of an Unmanned Surface Vehicle," *Journal of Field Robotics,* vol. 30, no. 3, p. 371–398, 2013.

[30]   G. H. Elkaim, "System identification-based control of an unmanned autonomous wind-propelled catamaran," *Control Engineering Practice,* vol. 17, no. 1, pp. 158-169, 2009.

[31]   The Maritime Safety Committee, *Resolution MSC.137(76) (adopted on 4 December 2002) Standards for Ship Manoeuvrability,* 2002.

[32]   I. Bertaska, Intelligent Supervisory Switching Control of Unmanned Surface Vehicles, Boca Raton: Florida Atlantic University, 2016.

[33]   T. Fossen and T. Johansen, "A Survey of Control Allocation Methods for Ships and Underwater Vehicles," in *14th Mediterranean Conference on Control and Automation, MED '06.* , Ancona, 2006.

[34]   T. Johansen, T. Fuglseth, P. Tøndel and T. Fossen, "Optimal constrained control allocation in marine surface vessels with rudders," *Control Engineering Practice,* vol. 16, no. 4, pp. 457-464, 2008.

[35]   T. Johansen, "Optimizing Nonlinear Control Allocation," in *43rd IEEE Conference on Decision and Control*, Paradise Island, Bahamas, 2004.

[36]   O. Sordalen, "Optimal Thrust Allocation for Marine Vessels," *Control Engineering Practice,* vol. 5, no. 9, pp. 1223-1231, 1997.

[37]   J. Newman, Marine Hydrodynamics, Cambridge, MA: The MIT Press, 1977.

[38]   M. Triantafyllou, "2.154 Maneuvering and Control of Surface and Underwater Vehicles (13.49), Fall 2004," (Massachusetts Institute of

Technology: MIT OpenCouseWare), http://ocw.mit.edu, (Accessed December 12, 2017). License: Creative Commons BY-NC-SA. [Online].

[39]   E. I. Sarda, H. Qu, I. R. Bertaska and K. D. von Ellenrieder, "Station-keeping control of an unmanned surface vehicle exposed to current and wind disturbances," *Ocean Engineering,* vol. 127, pp. 305-324, 2016.

[40]   "PID Controller, Discrete PID Controller," MathWorks, [Online]. Available: https://www.mathworks.com/help/simulink/slref/pidcontroller.html. [Accessed 21 March 2018].

[41]   R. C. Dorf and R. H. Bishop, Modern Control Systems, Eighth Edition, Menlo Park: Addison Wesley Longman, Inc., 1998.